ARTICLE

Cyclin B3 promotes anaphase I onset in oocyte meiosis

Mehmet E. Karasu[1,2,3]*, Nora Bouftas[4,5]*, Scott Keeney[1,2,3], and Katja Wassmann[4,5]

Meiosis poses unique challenges because two rounds of chromosome segregation must be executed without intervening DNA replication. Mammalian cells express numerous temporally regulated cyclins, but how these proteins collaborate to control meiosis remains poorly understood. Here, we show that female mice genetically ablated for cyclin B3 are viable—indicating that the protein is dispensable for mitotic divisions—but are sterile. Mutant oocytes appear normal until metaphase I but then display a highly penetrant failure to transition to anaphase I. They arrest with hallmarks of defective anaphase-promoting complex/cyclosome (APC/C) activation, including no separase activity, high CDK1 activity, and high cyclin B1 and securin levels. Partial APC/C activation occurs, however, as exogenously expressed APC/C substrates can be degraded. Cyclin B3 forms active kinase complexes with CDK1, and meiotic progression requires cyclin B3–associated kinase activity. Cyclin B3 homologues from frog, zebrafish, and fruit fly rescue meiotic progression in cyclin B3–deficient mouse oocytes, indicating conservation of the biochemical properties and possibly cellular functions of this germline-critical cyclin.

Introduction

Eukaryotic cell division depends on oscillations of CDKs associated with specific cyclins (Morgan, 1997; Malumbres et al., 2009; Uhlmann et al., 2011; Fisher et al., 2012). In vertebrate somatic cells, progression from G1 into S phase, G2, and mitosis depends on the cyclin D family, followed by the cyclin E, A, and B families (Morgan, 1997). Ordered CDK activity likewise governs progression through meiosis: chromosome condensation, congression, and alignment require a rise in cyclin B1–CDK1 activity, then anaphase onset is driven by inactivation of cyclin B1–CDK1 by the anaphase promoting complex/cyclosome (APC/C), an E3 ubiquitin ligase that targets substrates for degradation (Heim et al., 2017). Cyclin B1–CDK1 activity then reaccumulates, without DNA replicating again, while cyclin B1–CDK1 activity is low between meiosis I and II (Petronczki et al., 2003; El Yakoubi and Wassmann, 2017). Apart from cyclin B2, which can compensate for loss of cyclin B1 (Li et al., 2018a), the roles of specific cyclins in determining orderly meiotic progression remain poorly understood in mammalian oocytes.

Particularly enigmatic is cyclin B3, which forms a family distinct from other cyclins based on sequence alignments, but which contains structural motifs characteristic of both A- and B-type cyclins (Nieduszynski et al., 2002; Gunbin et al., 2011). Chicken cyclin B3 shows nuclear localization when ectopically expressed in HeLa cells, similar to A-type cyclins (Gallant and Nigg, 1994), but its orthologues cluster more closely with B-type

cyclins based on amino acid sequence (Nieduszynski et al., 2002; Gunbin et al., 2011). Cyclin B3 is conserved across metazoans (Lozano et al., 2012). Ciona intestinalis cyclin B3 counteracts zygotic transcription (Treen et al., 2018). In Xenopus laevis, no cyclin B3 protein was detected in oocytes or the first embryonic divisions (Hochegger et al., 2001), but whether cyclin B3 has a role at these stages has not been addressed. Drosophila melanogaster cyclin B3 is dispensable for mitotic divisions and male fertility but is essential for female fertility (Jacobs et al., 1998). In flies, cyclin B3 promotes anaphase onset in early embryonic divisions (Yuan and O'Farrell, 2015), and loss of cyclin B3 perturbs exit from meiosis I (Jacobs et al., 1998). Moreover, Drosophila cyclin B3 is degraded depending on the APC/C in mitosis, with later timing than cyclin A and B (Sigrist et al., 1995; Yuan and O'Farrell, 2015). Unlike in Drosophila (Yuan and O'Farrell, 2015), in Caenorhabditis elegans embryos, cyclin B3 appears to promote anaphase onset in meiosis II and mitosis via the spindle assembly checkpoint (SAC; van der Voet et al., 2009; Deyter et al., 2010). C. elegans and Drosophila cyclin B3 associate with CDK1 and support kinase activity in vitro (Jacobs et al., 1998; van der Voet et al., 2009).

Cyclin B3 protein is larger in placental mammals because of extension of a single exon (Lozano et al., 2012). Mouse cyclin B3 was proposed to promote recombination in male meiosis because its mRNA is present early in prophase I (Nguyen et al.,

[1]Molecular Biology Program, Memorial Sloan-Kettering Cancer Center, New York, NY; [2]Louis V. Gerstner Jr. Graduate School of Biomedical Sciences, Memorial Sloan-Kettering Cancer Center, New York, NY; [3]Howard Hughes Medical Institute, Memorial Sloan-Kettering Cancer Center, New York, NY; [4]Institut de Biologie Paris Seine, Sorbonne Université, Paris, France; [5]Developmental Biology Lab, Sorbonne Université, Centre National de la Recherche Scientifique UMR7622, Paris, France.

*M.E. Karasu and N. Bouftas contributed equally to this paper; Correspondence to Katja Wassmann: katja.wassmann@upmc.fr; Scott Keeney: s-keeney@ski.mskcc.org.

Check for updates

2002; Refik-Rogers et al., 2006). Prolonged cyclin B3 expression perturbed spermatogenesis and cyclin B3 interacted with CDK2, although no kinase activity was detected (Nguyen et al., 2002; Refik-Rogers et al., 2006). In females, cyclin B3 was speculated to govern meiotic initiation because its mRNA is up-regulated as oogonia cease proliferation and enter prophase I (Miles et al., 2010). RNAi-mediated knockdown of cyclin B3 by ∼70% in cultured oocytes perturbed meiosis I progression (Zhang et al., 2015). However, the molecular basis of the progression defect was not defined, and RNAi off-target effects could not be excluded, so cyclin B3 function remained unclear.

To sum up, cyclin B3 is implicated in female meiosis and early embryogenesis in different organisms, but its function is poorly understood, particularly in mammals. To gain insights into its potential roles, we generated mice with a targeted mutation in *Ccnb3*, the gene encoding cyclin B3. Mutant mice are viable, males are fertile, and oocytes enter meiosis. Strikingly, however, most mutant oocytes cannot progress beyond metaphase I, so *Ccnb3*-deficient female mice are sterile. Our data suggest that cyclin B3 fine-tunes APC/C activity toward meiotic substrates in oocyte meiosis I, at least in part as a partner enabling CDK1 catalytic activity, and that the biochemical function of cyclin B3 is conserved in vertebrates.

Results

Female mice are sterile after genetic ablation of *Ccnb3*

Ccnb3 spans 62 kb on the X chromosome and gives rise to a 4.1-kb mRNA of 14 exons encoding a 157.9-kD protein. CRISPR/Cas9 genome editing generated a 14-bp deletion at the 3′ end of the 2.7-kb-long exon 7, causing a frameshift and premature stop codon upstream of the cyclin box in exons 9–13 (Fig. 1 A). Immunoprecipitation/Western blotting of extracts from *Ccnb3*$^{-/Y}$ mutant testes yielded no signal for either full-length cyclin B3 or the predicted truncation product (1,090 amino acids, ∼123 kD; Fig. 1 B), indicating that the mutation is a null or severe loss-of-function allele.

Surprisingly, cyclin B3–deficient males were fertile, with no detectable meiotic abnormalities (the male phenotype will be described elsewhere). Heterozygous females had normal fertility, and homozygous mutant females were born in Mendelian frequencies (105 +/– [25.7%]: 100 –/– [25.5%]: 102 +/Y [25%]: 101 –/Y [24.8%] offspring from *Ccnb3*$^{+/-}$ females crossed with *Ccnb3*$^{-/Y}$ males). Cyclin B3–deficient animals displayed no gross abnormalities in major organs and tissues (Materials and methods), so cyclin B3 is dispensable in most if not all nonmeiotic cells.

Strikingly, however, mutant females were sterile. No pregnancies were observed, and no pups were born from *Ccnb3*$^{-/-}$ females (n = 9) bred with wild-type males for two rounds of mating. Thus, whereas cyclin B3 is dispensable for male meiosis, it is essential for female fertility.

Cyclin B3 is required for the metaphase-to-anaphase I transition in oocytes

Mammalian female meiosis initiates during fetal development (Herbert et al., 2015; El Yakoubi and Wassmann, 2017). Oocytes

complete chromosome pairing and recombination before birth, and then enter a prolonged arrest (the dictyate stage) and form primordial follicles, which are the resting pool of germ cells that will be recruited later for ovulation. *Ccnb3*$^{-/-}$ ovary sections showed abundant primordial and growing follicles at 2–3 mo of age and were quantitatively and morphologically indistinguishable from controls (Fig. 1 C). Mutations compromising oogonial development, meiotic initiation, or recombination cause drastically reduced or absent follicles (Di Giacomo et al., 2005; Baltus et al., 2006; Li and Schimenti, 2007; Bolcun-Filas et al., 2014; Jain et al., 2018). The normal number of follicles in *Ccnb3*$^{-/-}$ females therefore implies that cyclin B3 is dispensable for germ cell divisions before meiosis and for early events of meiotic prophase I.

We next tested the ability of mutant oocytes to enter meiosis I and to divide. Germinal vesicle (GV) stage oocytes from adult *Ccnb3*$^{-/-}$ mice and age-matched controls from the same breedings (*Ccnb3*$^{+/-}$) were cultured in vitro. Germinal vesicle breakdown (GVBD; corresponding to nuclear envelope breakdown in mitosis) occurred with normal timing (within 90 min) and efficiency in *Ccnb3*$^{-/-}$ oocytes (Fig. 1 D); thus, cyclin B3 is dispensable for entry into meiosis I. At ∼7–10 h in culture after GVBD, depending on the mouse strain, oocytes extrude a polar body (PB), indicating execution of the first division and exit from meiosis I (Holt et al., 2013; El Yakoubi and Wassmann, 2017). *Ccnb3*$^{-/-}$ mice had a highly penetrant defect: oocytes from most mutant mice failed to extrude a PB (71 of 79 mice; Fig. 1 D). These findings indicate that cyclin B3 is required for progression through meiosis I and that meiotic progression failure is the cause of female infertility. Because penetrance of meiotic arrest was mouse specific (i.e., most mice yielded only arrested oocytes), we focused on the large majority of mice in which no PB extrusion was observed. (For every *Ccnb3*$^{-/-}$ mouse, a fraction of oocytes was matured in the incubator and left untreated to verify that no PB extrusion occurred; see Materials and methods.) Possible reasons for incomplete penetrance are addressed in the Discussion.

To further characterize arrest, we followed meiotic progression by live imaging. GV oocytes were injected with mRNA encoding histone H2B fused to RFP and β-tubulin fused to GFP to visualize chromosomes and spindles, respectively. Whereas control oocytes separated their chromosomes and extruded PBs ∼8 h after GVBD, *Ccnb3*$^{-/-}$ oocytes remained in a metaphase I–like state, with a spindle that had migrated to the cortex and chromosomes aligned at the spindle midzone (Fig. 2 A and Videos 1 and 2).

Hypothesizing that mutant oocytes were failing to transition to anaphase I, we predicted that homologous chromosomes would still be conjoined in arrested oocytes. Chromosome spreads from controls had the expected 20 bivalent chromosomes (homologue pairs connected by chiasmata) before the first division (6 h after GVBD) and pairs of sister chromatids juxtaposed near their centromeres afterward (metaphase II arrest, 16 h after GVBD; Fig. 2 B). In contrast, *Ccnb3*$^{-/-}$ oocytes had intact bivalents with no homologue separation throughout the arrest in culture, indicating a metaphase I arrest (Fig. 2 B).
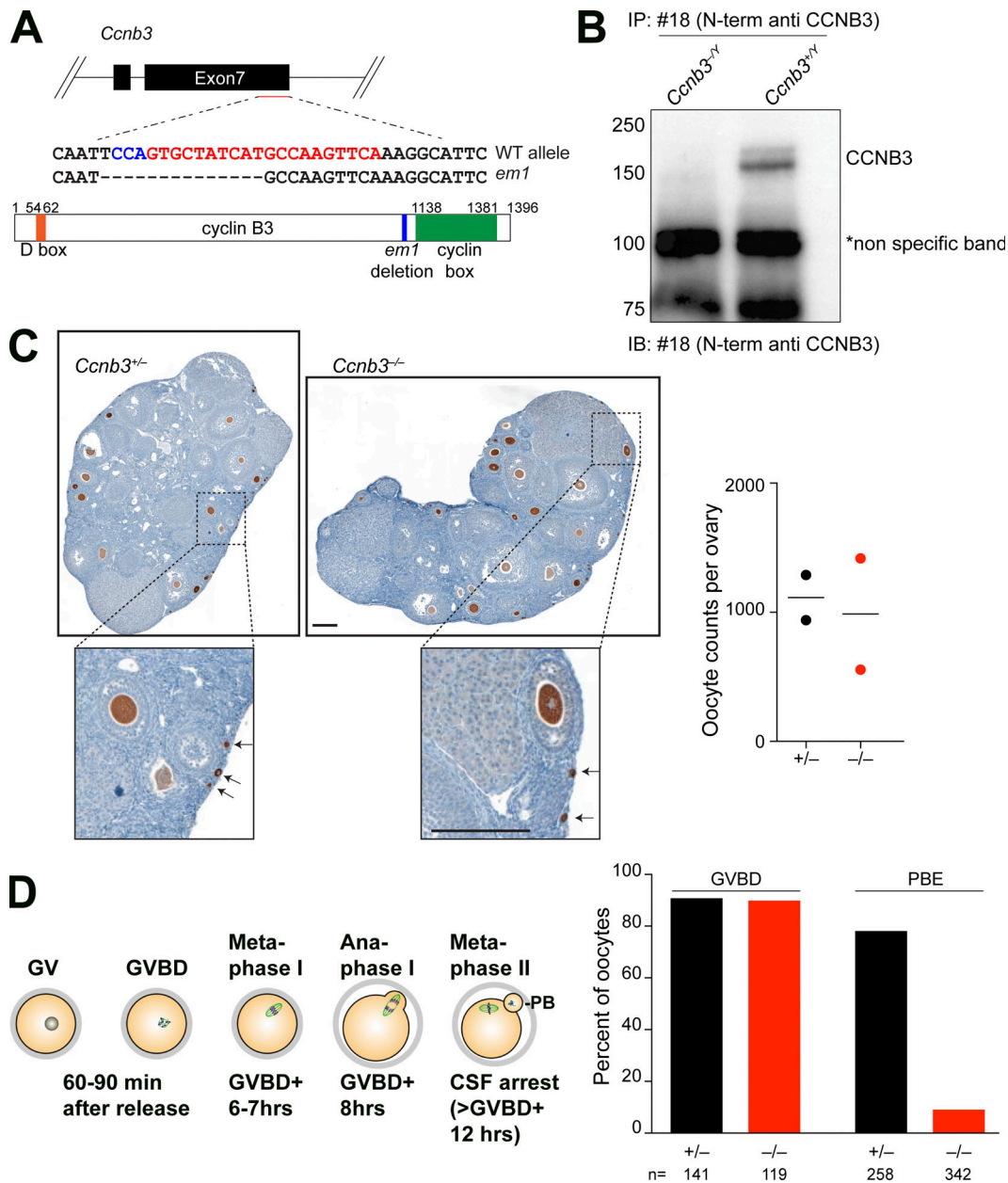
Figure 1. **Generation of *Ccnb3*⁻/⁻ mice reveals a requirement for cyclin B3 in female meiosis. (A)** Targeted mutation of *Ccnb3*. Top: Exons 6 and 7 are shown as black rectangles. A portion of the sequences of the wild-type allele and *em1* mutant allele are shown, with guide RNA position in red and the complement of the protospacer adjacent motif (PAM) sequence in blue. Bottom: Schematic of cyclin B3 protein. **(B)** Immunoprecipitation and Western blot analysis of adult testis extracts using an anti–cyclin B3 monoclonal antibody. **(C)** Apparently normal folliculogenesis and oocyte reserves in *Ccnb3*-deficient females. Left: PFA-fixed, anti-MVH–stained ovary sections from 3-mo-old animals. Zoomed images show presence of primary/primordial follicles indicated by black arrows. Scale bars, 500 µm. Right: Oocyte counts from two 3-mo-old females of each genotype. PFA-fixed ovaries were sectioned completely and stained with anti-MVH. Stained oocytes were counted in every fifth ovary section and summed. Each point is the count for one ovary of one animal; means are 1,114 for *Ccnb3*⁺/⁻ and 987 for *Ccnb3*⁻/⁻. **(D)** The scheme illustrates progression through the meiotic divisions until metaphase II arrest in oocytes of the mouse strain used. The graph on the right shows percentages of mature oocytes of the indicated genotypes that underwent GVBD within 90 min in culture after release, and oocytes that extruded PBs. n: total number of oocytes counted in >10 independent experiments (GVBD: 141% *Ccnb3*⁺/⁻: 90.78%; 119 *Ccnb3*⁻/⁻: 89.91%; PB extrusion (PBE): 258 *Ccnb3*⁺/⁻: 78.13%; 342 *Ccnb3*⁻/⁻: 9.06%).

Arrest was not due to failure in forming spindles or stable kinetochore–microtubule interactions, because metaphase I spindles displayed no obvious morphological defects and cold-stable microtubule fibers were comparable to control oocytes in metaphase I (Fig. 2 C). Microtubule fibers attached to kinetochores were clearly visible, so cyclin B3 is not required for kinetochore–microtubule attachments (Fig. 2 C). Spindles in *Ccnb3*⁻/⁻ oocytes retained the barrel shape characteristic of metaphase I even at late time points 16 h after GVBD, when control oocytes had progressed to metaphase II, with elongated spindles and more focused spindle poles (Fig. 2 C).
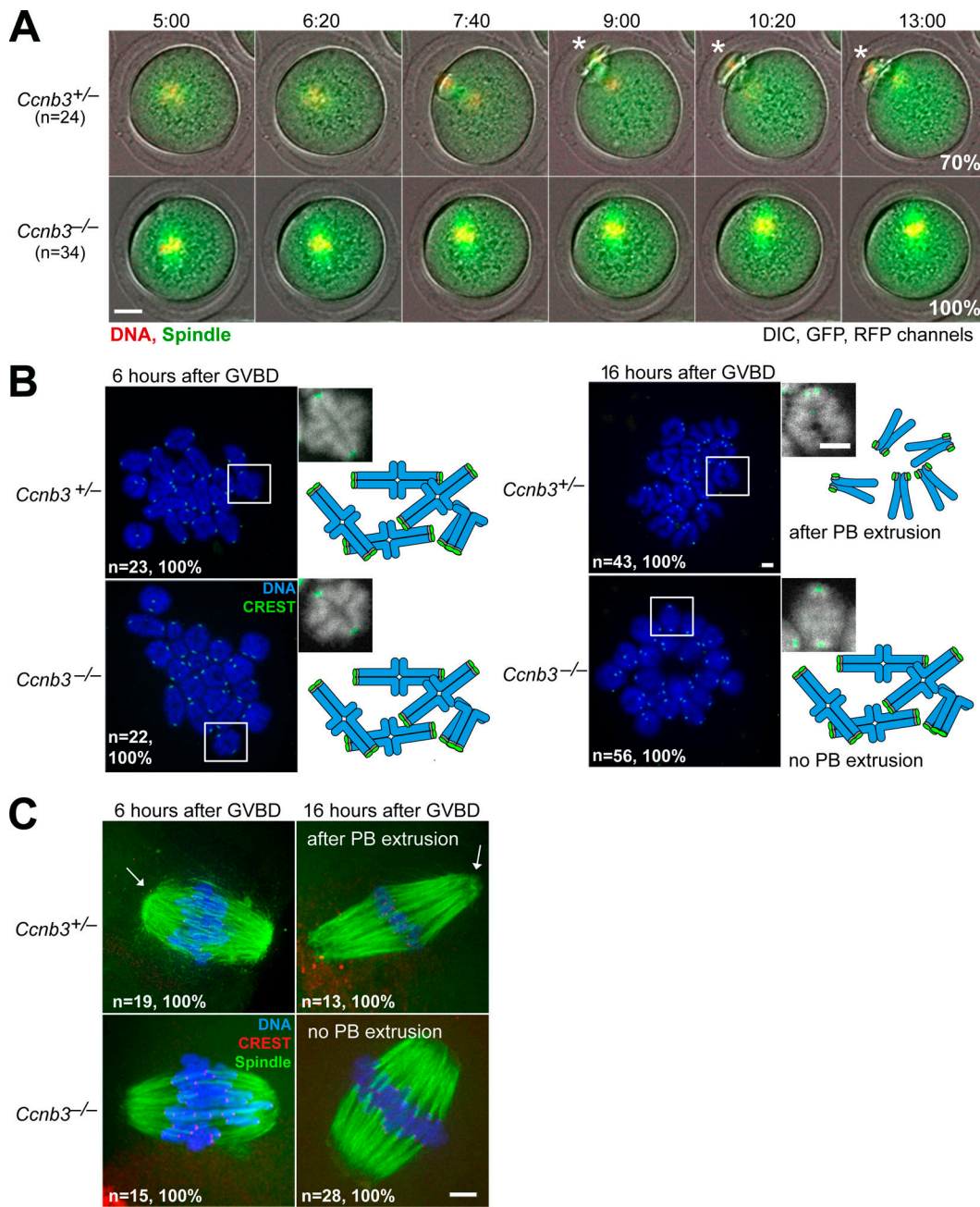
Karasu et al.
Role of cyclin B3 in oocyte meiosis I

Journal of Cell Biology 1267
https://doi.org/10.1083/jcb.201808091

Figure 2. **Cyclin B3 is required for the metaphase-to-anaphase I transition in oocytes. (A)** Live-cell imaging of meiotic maturation. β-Tubulin-GFP and H2B-RFP mRNA, used to visualize spindle and chromosomes, were injected into GV-stage oocytes, which were then induced to enter meiosis I. Selected time frames are shown, with overlay of DIC, GFP, and RFP channels of collapsed z-sections (11 section, 3-μm steps) from a representative video. Time after GVBD is indicated as hours:minutes. n: number of oocytes analyzed. Percentage of oocytes of the observed phenotype from two independent experiments is indicated. White asterisks indicate PBs. Scale bar, 20 μm. Related to Videos 1 and 2. **(B)** Chromosome spreads 6 h (corresponding to metaphase I) and 16 h (corresponding to metaphase II in controls) after GVBD. Kinetochores were stained with CREST (green) and chromosomes with Hoechst (blue). Insets show typical chromosome figures observed; for better visualization, chromosomes are shown in grayscale. Schematics of metaphase I bivalents or metaphase II univalent chromosomes are shown to aid interpretation. Scale bar, 5 μm. n: number of oocytes analyzed in three independent experiments. **(C)** Whole-mount immunofluorescence staining of cold-treated spindles. Microtubules were stained with anti-tubulin antibody (green), kinetochores with CREST (red), and chromosomes with Hoechst (blue). Spindle poles typical of metaphase I and metaphase II are indicated with arrows in controls. Scale bar, 5 μm. n: number of oocytes analyzed in three independent experiments.

Arrest in $Ccnb3^{-/-}$ oocytes is accompanied by incomplete degradation of APC/C substrates

Separase is a cysteine protease that cleaves the kleisin subunit of cohesin complexes to dissolve sister chromatid cohesion at anaphase onset in mitosis and meiosis (Stemmann et al., 2006). Before anaphase, separase activity is restrained in part by binding to its inhibitory chaperone, securin, and by high cyclin B–CDK activity (Stemmann et al., 2006). In oocytes,

APC/C-dependent degradation of securin and cyclin B1 activates separase, which cleaves the meiotic kleisin REC8, allowing homologous chromosomes to separate (Herbert et al., 2003; Terret et al., 2003; Kudo et al., 2006). To follow separase activity in live oocytes, we expressed a separase activity sensor (Nikalayevich et al., 2018), similar to one used in cultured mitotic cells (Shindo et al., 2012). The sensor harbors two fluorescent tags separated by a fragment of mitotic kleisin RAD21 as a separase substrate; this ensemble is fused to histone H2B to localize it to chromosomes. Cleavage by separase leaves only the H2B-attached fluorophore on chromosomes (Fig. 3 A). Sensor cleavage occurs only under conditions when endogenous REC8 is removed from chromosome arms (Nikalayevich et al., 2018). In control oocytes, the fluorescent signal on chromosomes changed abruptly from yellow to red upon anaphase onset (Fig. 3 B, top row, compare 6:20 to 6:40). In contrast, both fluorophores remained chromatin-associated throughout arrest in *Ccnb3⁻/⁻* oocytes (Fig. 3 B, bottom row), indicating that separase cannot be activated and explaining why mutant oocytes cannot separate homologous chromosomes and extrude PBs.

Failure to activate separase was potentially due to a failure to degrade cyclin B1 and securin, so we analyzed each protein by Western blotting (Fig. 3 C). In control oocytes, levels of both proteins decreased precipitously at anaphase onset (compare 8:30 to 3:30 after GVBD). In *Ccnb3⁻/⁻* oocytes, in contrast, cyclin B1 levels did not decrease, even at late times. In fact, cyclin B1 levels were consistently higher during arrest (8:30 and later) than in prometaphase (3:30). Securin levels decreased between 3:30 and 8:30 after GVBD, but remained higher than in the controls. Thus, although securin levels drop partially, both proteins are inappropriately stabilized at the time the meiosis I division would normally be performed.

Next, we asked whether cyclin B1 stabilization led to elevated kinase activity in extracts from cultured oocytes. Phosphorylation of histone H1 in vitro is mostly attributable to CDK1 plus cyclin B1 (Kubiak et al., 1992; Morgan, 1997; Malumbres et al., 2009; Fig. 3 D). Control oocytes showed high H1 kinase activity in metaphase I (6:00 after GVBD) and a drop in kinase activity when they extruded PBs (8:00 after GVBD; Ledan et al., 2001). *Ccnb3⁻/⁻* oocytes showed high kinase activity in metaphase I (6:00 after GVBD), but no drop in kinase activity was observed at the time when normal cells extruded PBs (8:00 after GVBD; Fig. 3 D). These findings suggest that persistence of high cyclin B1 levels in the mutant maintains high CDK1 activity.

Because endogenous securin decreased slightly in *Ccnb3⁻/⁻* oocytes (Fig. 3 C), whereas cyclin B1 and H1 kinase activity did not (Fig. 3, C and D), we asked whether inhibiting CDK activity at the normal time of anaphase I onset would suffice for *Ccnb3⁻/⁻* oocytes to undergo anaphase I and PB extrusion. Indeed, the CDK inhibitor roscovitine (Meijer et al., 1997) rescued PB extrusion and chromosome segregation, suggesting that meiotic arrest is mainly due to persistently elevated cyclin B1–CDK1 activity (Fig. 3 E).

The results thus far led us to conclude that *Ccnb3⁻/⁻* oocytes arrest in metaphase I with aligned bivalents, bipolar spindles, high securin and cyclin B1 protein levels, and little or no separase activity. In oocytes, degradation of cyclin B1 and securin depends on ubiquitination by the APC/C (Herbert et al., 2003; Terret et al., 2003). Hence, our results suggested that without cyclin B3, the APC/C is not sufficiently activated, but because endogenous securin levels did decrease slightly, we suspected that the APC/C might be partially active. To test this, we asked whether exogenously expressed securin and cyclin B1 were also stabilized by live imaging of oocytes injected with mRNAs coding for either protein fused to fluorescent tags (Herbert et al., 2003; Kudo et al., 2006; Niault et al., 2007; Gui and Homer, 2012; Lane et al., 2012; Rattani et al., 2014). Surprisingly, cyclin B1–GFP and securin-YFP were both efficiently degraded in *Ccnb3⁻/⁻* oocytes (Fig. 3 F). Securin-YFP was degraded with kinetics and final extent similar to the controls, whereas cyclin B1–GFP appeared to be degraded slightly more slowly and was higher in *Ccnb3⁻/⁻* specifically at the time controls underwent PB extrusion (Fig. 3 F). Thus, even though both exogenous substrates were more efficiently degraded than their endogenous counterparts, the differences between the two substrates were similar in both contexts (i.e., securin was degraded to a greater extent than cyclin B1 in the absence of cyclin B3). These results indicate that the APC/C indeed becomes partially active in the mutants, but further suggest that cyclin B3 specifically promotes degradation of endogenous APC/C substrates. This may be by modulating APC/C specificity, per se, or by regulating the substrates or their localization to affect their ability to be ubiquitinated.

Timely APC/C activation depends on satisfaction of the SAC (Holt et al., 2013; Touati and Wassmann, 2016), so we asked whether inappropriate SAC activity was the reason for arrest in *Ccnb3⁻/⁻* oocytes. Kinetochore recruitment of SAC components, such as MAD2, is a readout for SAC activation (Wassmann et al., 2003; Gui and Homer, 2012; Lischetti and Nilsson, 2015). Similar to controls, MAD2 was recruited to unattached kinetochores early in meiosis I and was not abnormally retained in metaphase I in *Ccnb3⁻/⁻* oocytes (Fig. 4 A). We further treated *Ccnb3⁻/⁻* oocytes with reversine, which inhibits the SAC kinase MPS1 (Santaguida et al., 2010). Reversine overcame nocodazole-induced arrest in control cells as previously shown (Touati et al., 2015) but did not rescue metaphase arrest caused by cyclin B3 deficiency (Fig. 4 B). We conclude that prolonged SAC activation is not the reason for metaphase I arrest and failure to efficiently degrade endogenous APC/C substrates.

Exogenously expressed cyclin B3 is an APC/C substrate in meiosis

Like other M-phase cyclins, cyclin B3 has a destruction box (D-box; Nguyen et al., 2002), a motif for APC/C-dependent ubiquitination (Yuan and O'Farrell, 2015; Fig. 1 A). In mitosis, exogenous cyclin B3 is degraded after cyclin B1 (Nguyen et al., 2002), so we asked about cyclin B3 stability in oocytes. mRNA encoding cyclin B3–RFP was injected into wild-type oocytes together with mRNA for either securin-YFP or cyclin A2-GFP, and oocytes were followed by live imaging. Cyclin B3–RFP accumulated during meiosis I, then was degraded abruptly just before PB extrusion. Importantly, cyclin B3 was degraded after both cyclin A2 and securin (Fig. 5, A and B), showing temporally ordered degradation of APC/C substrates in oocyte meiosis I, at
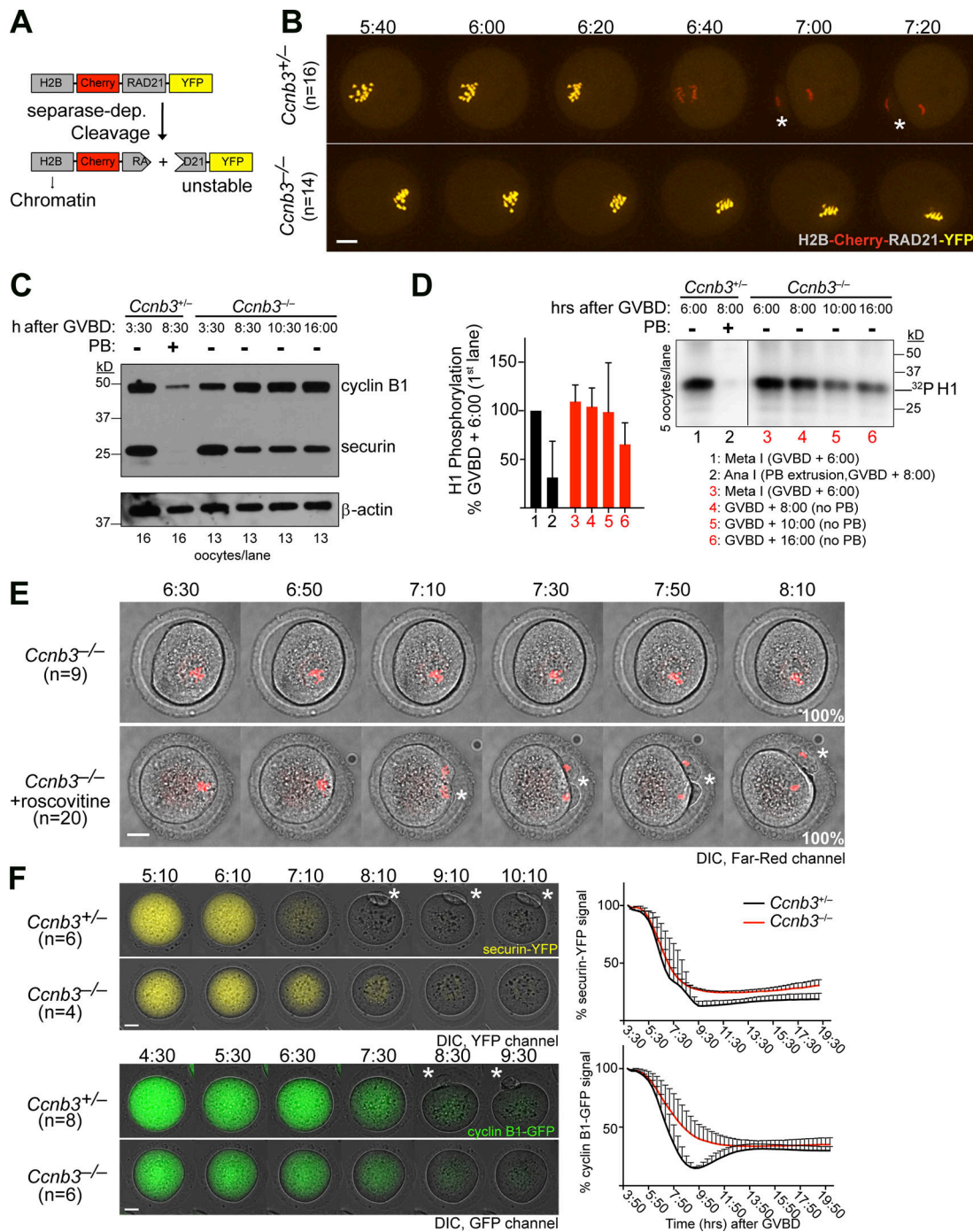
Karasu et al.
Role of cyclin B3 in oocyte meiosis I

Journal of Cell Biology
https://doi.org/10.1083/jcb.201808091

1269

Figure 3. **Cell cycle arrest in *Ccnb3*⁻/⁻ oocytes is associated with incomplete APC/C activation. (A)** Schematic of separase activity sensor. See text for details. **(B)** Failure to activate separase in the absence of cyclin B3. Separase activity sensor mRNA was injected into GV oocytes, which were released into meiosis I and visualized by spinning-disk confocal microscopy. Selected time frames of collapsed z-sections (11 sections, 3-µm steps) from a representative video are shown. Time points after GVBD are indicated as hours:minutes. Scale bar, 20 µm. White asterisks indicate PBs. n: number of oocytes from three independent experiments. **(C)** Western blot analysis of cyclin B1 and securin during oocyte maturation, at the time points, indicated as hours:minutes after GVBD. β-Actin served as the loading control. The number of oocytes used and the presence or absence of a PB are indicated. Two mice of each genotype were used per experiment. The data shown are representative of results from two independent experiments. **(D)** Total cyclin B–CDK1 activity during oocyte maturation, at the time points indicated as hours:minutes after GVBD. Histone H1 was used as a substrate. Five oocytes were used per kinase reaction; presence or absence of a PB is indicated. The graph shows quantification of phosphate incorporation from three independent experiments, and error bars indicate SD (means ± SD: lane 1: 100 [used for normalization]; lane 2: 31.27 ± 37.28; lane 3: 109.34 ± 17.09; lane 4: 104.05 ± 19.33; lane 5: 98.67 ± 50.56; lane 6: 65.40 ± 22.12). **(E)** CDK inhibition rescues meiosis I division. Oocytes were incubated with siR-DNA to visualize chromosomes. In metaphase I, 6 h 20 min after GVBD, oocytes were treated with 0.2 mM roscovitine (final concentration), where indicated, and the video was started. Selected time frames of collapsed z-sections (11 sections, 3-µm steps) of DIC far-red channel from a representative movie of *Ccnb3*⁻/⁻ oocytes with or without roscovitine treatment are shown. The asterisk indicates chromosome segregation in anaphase I. Time points after GVBD are indicated as hours:minutes. Scale bar: 20 µm. n: number of oocytes

from three independent experiments. **(F)** Degradation of exogenous APC/C substrates. Securin-YFP (top) or cyclin B1–GFP (bottom) mRNA was injected into GV oocytes. Stills from representative videos are shown. Time points after GVBD are indicated as hours:minutes. Scale bar, 20 µm. n: number of oocytes from two independent experiment); white asterisk indicates PB extrusion (PBE). Fluorescence intensities (mean ± SD) were quantified from the indicated number of oocytes imaged (securin-YFP: 4 *Ccnb3*⁻/⁻, 6 *Ccnb3*⁺/⁻; cyclin B1–GFP injections: 6 *Ccnb3*⁻/⁻, 8 *Ccnb3*⁺/⁻).

least for exogenous proteins. No reaccumulation of cyclin B3-RFP was observed in meiosis II. Deleting the D-box stabilized cyclin B3–RFP (Fig. 5 C; there is no obvious KEN-box or ABBA motif; Davey and Morgan, 2016). These findings support the conclusion that cyclin B3 is an APC/C substrate in oocytes.

Cyclin B3–associated kinase activity is required for progression through oocyte meiosis I

To test whether mouse cyclin B3 supports CDK1 kinase activity as for *C. elegans*, *Drosophila*, and chicken proteins (Gallant and Nigg, 1994; Jacobs et al., 1998; van der Voet et al., 2009), we expressed and purified from insect cells cyclin B3 N-terminally tagged with maltose binding protein (MBP) and hexahistidine (^MBPHis^cyclin B3) plus untagged or HA-tagged CDK1. Both CDK1 and CDK1-HA copurified with ^MBPHis^cyclin B3 on amylose resin (Fig. 6 A, left, lanes 2 and 3), and both cyclin B3–CDK1 complexes displayed kinase activity toward histone H1 in vitro (Fig. 6 A, right, lanes 2 and 3).

To investigate this kinase activity, we mutated the conserved MRAIL motif on the cyclin fold (Jeffrey et al., 1995; Schulman et al., 1998). MRAIL mutations can prevent binding of cyclin–CDK complexes to substrates without affecting cyclin–CDK interactions (Schulman et al., 1998) or can disrupt cyclin–CDK interaction (Bendris et al., 2011). Mutating the methionine, arginine, and leucine residues of the MRAIL motif to alanine (cyclin B3–MRL mutant) did not affect copurification of CDK1 (Fig. 6 A, left, lanes 5 and 6) but eliminated kinase activity (Fig. 6 A, right, lanes 5 and 6). Furthermore, purification of wild-type cyclin B3 without coexpressed CDK1 yielded detectable kinase activity, presumably attributable to cyclin B3 association with one or more endogenous insect cell CDKs, but the MRL mutant gave no such activity (Fig. 6 A, right, lanes 1 and 4). Thus, cyclin B3 can form an active kinase complex with CDK1, suggesting in turn that CDK1 is a physiological partner. We also conclude that the MRL mutant permits CDK1 binding but abolishes associated kinase activity.

We further tested whether oocyte division requires cyclin B3–associated kinase activity. To this end, we first live-imaged *Ccnb3*⁻/⁻ oocytes injected with mRNA encoding wild-type or D-box–deleted (ΔDbox) cyclin B3. Both constructs efficiently rescued PB extrusion (Fig. 6 B). Rescue of MI division by the ΔDbox mutant demonstrated that cyclin B3 degradation is dispensable for anaphase I, and also led us to infer that exogenously expressed cyclin B3 was a quantitatively minor contributor to total CDK1 activity, because high CDK1 should prevent anaphase I. To confirm this idea, we examined H1 kinase activity in synchronized oocytes before and after PB extrusion in rescue experiments. Indeed, *Ccnb3*⁻/⁻ oocytes rescued by expression of wild-type or ΔDbox cyclin B3 did not show elevated H1 kinase activity in anaphase I (Fig. 6 C, compare lanes 3, 7, and 9). Interestingly though, we found less H1 kinase activity in

metaphase I oocytes expressing ΔDbox cyclin B3 (Fig. 6 C, lanes 4, 6, and 8), suggesting that cyclin B1–associated CDK1 kinase activity might be partially down-regulated by stable cyclin B3.

Separation of homologous chromosomes was also rescued upon cyclin B3 expression (Fig. 6 D), confirming that meiotic arrest is due to absence of cyclin B3 per se and establishing feasibility of structure/function experiments via complementation. In striking contrast to wild-type cyclin B3, the MRL mutant was unable to rescue meiosis I division, PB extrusion, or chromosome segregation (Fig. 6, B and D), indicating that cyclin B3–CDK complexes (likely CDK1) bring about anaphase I onset through their kinase activity toward yet unknown substrates. Note that, unlike cyclin B3, exogenous cyclin B1 did not rescue PB extrusion (Fig. 3 F) or homologue disjunction (Fig. 6 D).

Cyclin B3–CDK1 substrates are likely distinct from cyclin B1–CDK1 substrates, perhaps owing to different substrate specificity or accessibility. Furthermore, even though cyclin B3–CDK1 kinase activity is required for PB extrusion, its effect is probably locally restricted and does not lead to a detectable overall increase of CDK1 activity, at least as measured on histone H1 as a substrate.

Functional conservation of vertebrate cyclin B3 in meiosis I

It was previously reported that *X. laevis* oocytes have cyclin B3 mRNA but not detectable protein, from which it was inferred that cyclin B3 plays no role in *X. laevis* oocyte meiosis (Hochegger et al., 2001). Furthermore, cyclin B3 is much larger in mammals than in nonmammalian vertebrates owing to the extended exon 7 (Lozano et al., 2012), suggesting that the mammalian protein might be functionally distinct. To explore this possibility, we tested for interspecies cross-complementation by injecting mRNAs encoding either *X. laevis* or zebrafish (*Danio rerio*) cyclin B3 into mouse *Ccnb3*⁻/⁻ oocytes. Remarkably, heterologous expression of cyclin B3 from either species efficiently rescued PB extrusion (Fig. 7 A). Live imaging showed no obvious defect in chromosome alignment or anaphase I onset in oocytes rescued with *X. laevis* cyclin B3 (Fig. 7 B). The extended exon 7 in mouse cyclin B3 is thus dispensable to promote anaphase I onset. We further infer that cyclin B3 biochemical functions are conserved across vertebrates, in turn raising the possibility that cyclin B3 promotes the oocyte meiosis I division throughout the vertebrate lineage. Even more remarkably, *Drosophila* cyclin B3 was also able to rescue (Fig. 7 A), suggesting conservation of biochemical properties throughout metazoa.

Discussion

Whereas male fertility is unaffected by reduction (Tang et al., 2018) or complete loss (unpublished data) of cyclin B3, mutant
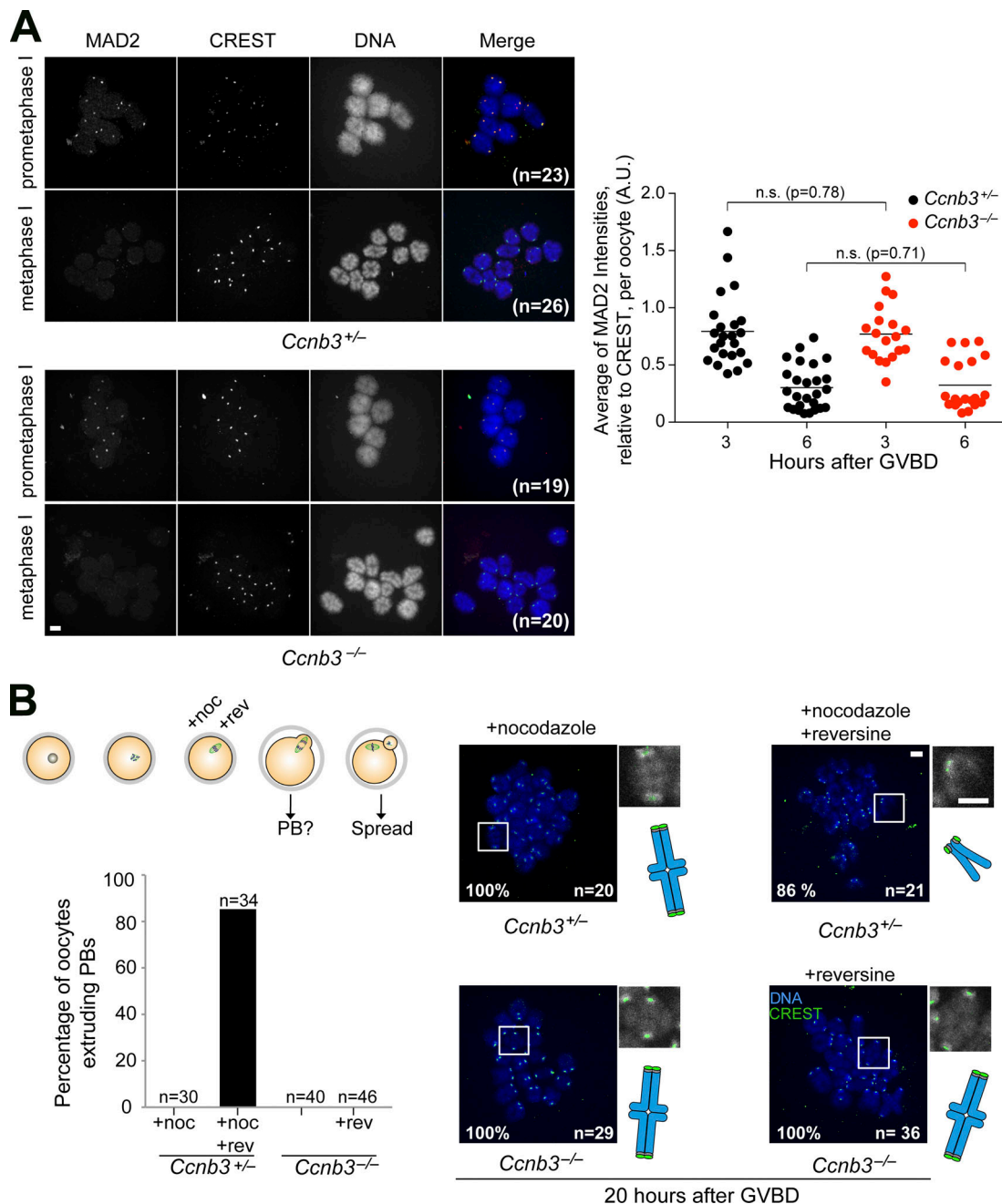
Figure 4. **SAC activation is not the cause of metaphase I arrest in *Ccnb3*⁻/⁻ oocytes. (A)** Left: Chromosome spreads were prepared 3 h (early prometaphase I) and 6 h (metaphase I) after GVBD, then stained with Hoechst (blue), CREST (green), and anti-MAD2 (red). Scale bar, 5 μm. Right: Quantification of MAD2 signal intensity relative to CREST; each point is the mean relative intensity averaged across centromeres in an oocyte. n: number of oocytes from three independent experiments. P values are from t tests. Number and means of oocytes stained 3 h after GVBD: 23 *Ccnb3*+/⁻ (mean: 0.794) and 19 *Ccnb3*⁻/⁻ (mean: 0.77); 6 h after GVBD: 26 *Ccnb3*+/⁻ (mean: 0.302) and 20 *Ccnb3*⁻/⁻ (mean: 0.325). **(B)** Oocytes were treated with reversine to override a potential SAC arrest. Control oocytes were treated with nocodazole from 6 h after GVBD onward, whereas *Ccnb3*⁻/⁻ oocytes were allowed to arrest without nocodazole. 6 h 40 min after GVBD, reversine was added, PB extrusion was scored visually (graph on the right, n: number of oocytes scored per genotype. 0% of oocytes extruded PBs, except oocytes treated with nocodazole and reversine, which extruded PBs in 85.29% of oocytes analyzed), and all oocytes were spread 20 h after GVBD. Kinetochores were stained with CREST (green) and chromosomes with Hoechst (blue). Insets show typical chromosome figures observed. Scale bar, 5 μm. n: the number of spreads from three independent experiments that allowed to unambiguously distinguish bivalents from univalents; percentage of oocytes with same phenotype is indicated.

females are sterile because cyclin B3 promotes degradation of APC/C substrates and thus triggers anaphase onset in the first meiotic division in oocytes. Similar findings were obtained with a different *Ccnb3* mutation (Li et al., 2018b *Preprint*). Our findings

definitively establish a crucial role for mouse cyclin B3 in the female germline.

The requirement in anaphase I onset is similar to *Drosophila* oocytes (Deyter et al., 2010; Yuan and O'Farrell, 2015). It was
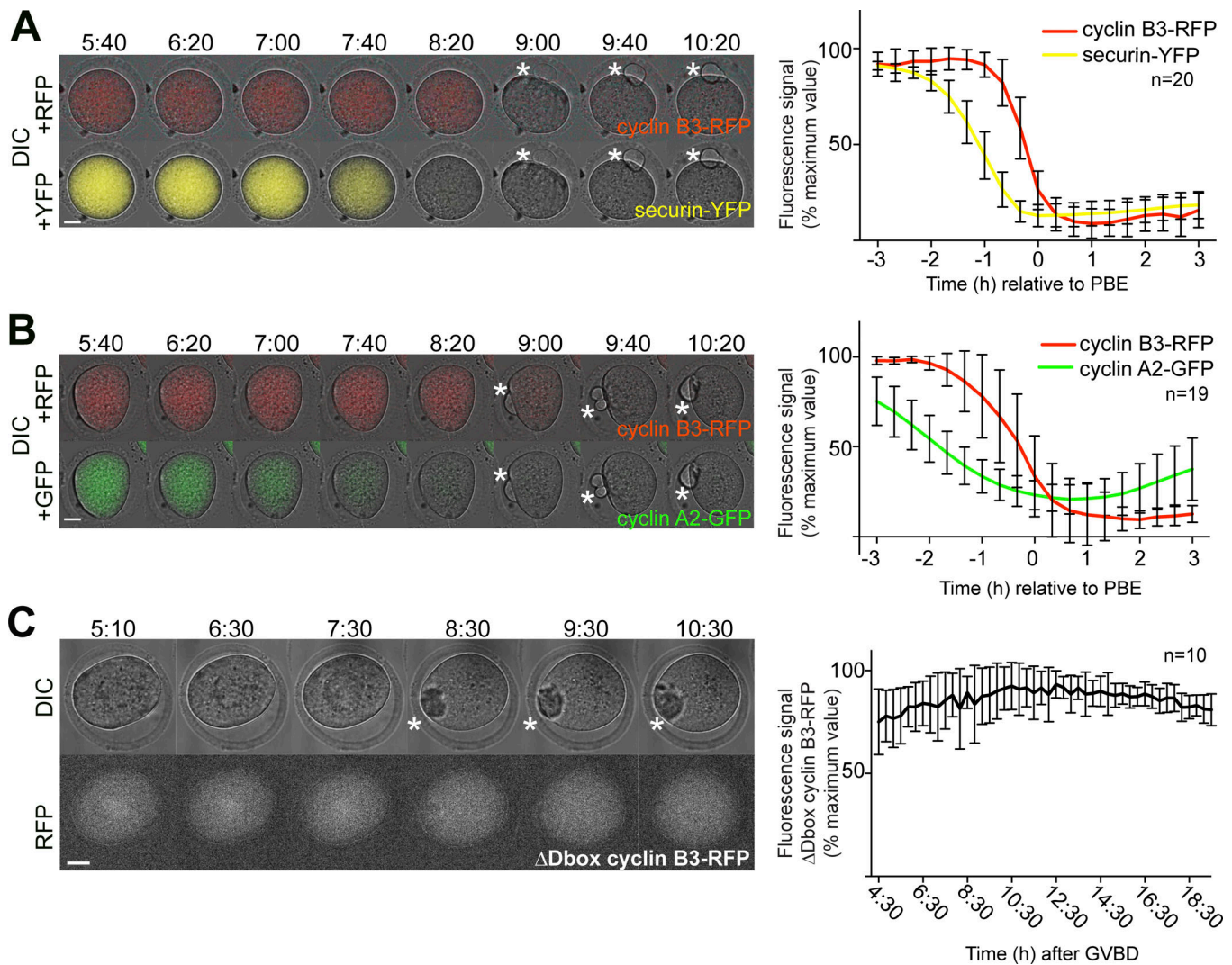
Figure 5. **Ordered degradation of APC/C substrates in oocyte meiosis I. (A and B)** Cyclin B3 was degraded after securin or cyclin A2. mRNA encoding cyclin B3–RFP and either securin-YFP (A; 20 oocytes) or cyclin A2–GFP (B; 19 oocytes) were coinjected into GV oocytes of CD-1 mice. Each panel shows selected frames from a video of a representative oocyte, with an overlay of DIC and RFP channels in the top rows, and DIC and YFP or GFP channels in the bottom rows. **(C)** The D box of cyclin B3 is required for degradation. CD-1 GV oocytes (10 oocytes) were injected with mRNA encoding cyclin B3–RFP with the D box deleted (ΔDbox). Frames from a representative video are shown, with the DIC channel on top and RFP at the bottom. All panels: Time points after GVBD (BD) are indicated as hours:minutes. Scale bars, 20 µm. White asterisks: PBs. Quantification of fluorescence intensities is shown on the right (mean ± SD of the indicated number of oocytes from three independent experiments).

proposed that cyclin B3 regulates APC/C activity during the rapid mitotic cycles of the early *Drosophila* embryo (Yuan and O'Farrell, 2015). Our data are consistent with a similar role in mouse oocyte meiosis I. Interestingly, however, exogenous APC/C targets are degraded efficiently in cyclin B3–deficient oocytes, but endogenous substrates are not, to our knowledge, the first such discrepancy observed. What distinguishes exogenous from endogenous substrates is not clear. One possibility is that expression timing (starting upon mRNA injection into GV oocytes) places exogenous proteins at a disadvantage for binding to essential partners, e.g., of securin to separase and cyclin B1 to CDK. It is also possible that fluorescent protein tags interfere slightly with this binding. Notably, free securin is degraded earlier than separase-bound securin, which is stabilized by maintenance in a nonphosphorylated state through association with phosphatase PP2A (Hellmuth et al., 2014). Securin phosphorylation enhances its affinity for the APC/C (Holt et al., 2008; Hellmuth et al., 2014), and cyclin B3 may control this step. Regardless of the source of the distinction, our data clearly demonstrate that APC/C becomes at least partially active on time, but may not be sufficiently active to robustly provoke degradation of all of its targets.

Alternatively, cyclin B3 may play a repressive role in translation of APC/C substrates after meiosis I entry. After GVBD, cyclin B1 and cyclin B2 mRNA association with polysomes is regulated in a distinct manner in mouse oocytes, resulting in translation of cyclin B1 transcripts but not cyclin B2 (Han et al., 2017). Translational control is crucial because oocytes contain stockpiles of mRNAs required for early embryo development, which are not required during oocyte meiosis (Yang et al., 2017).
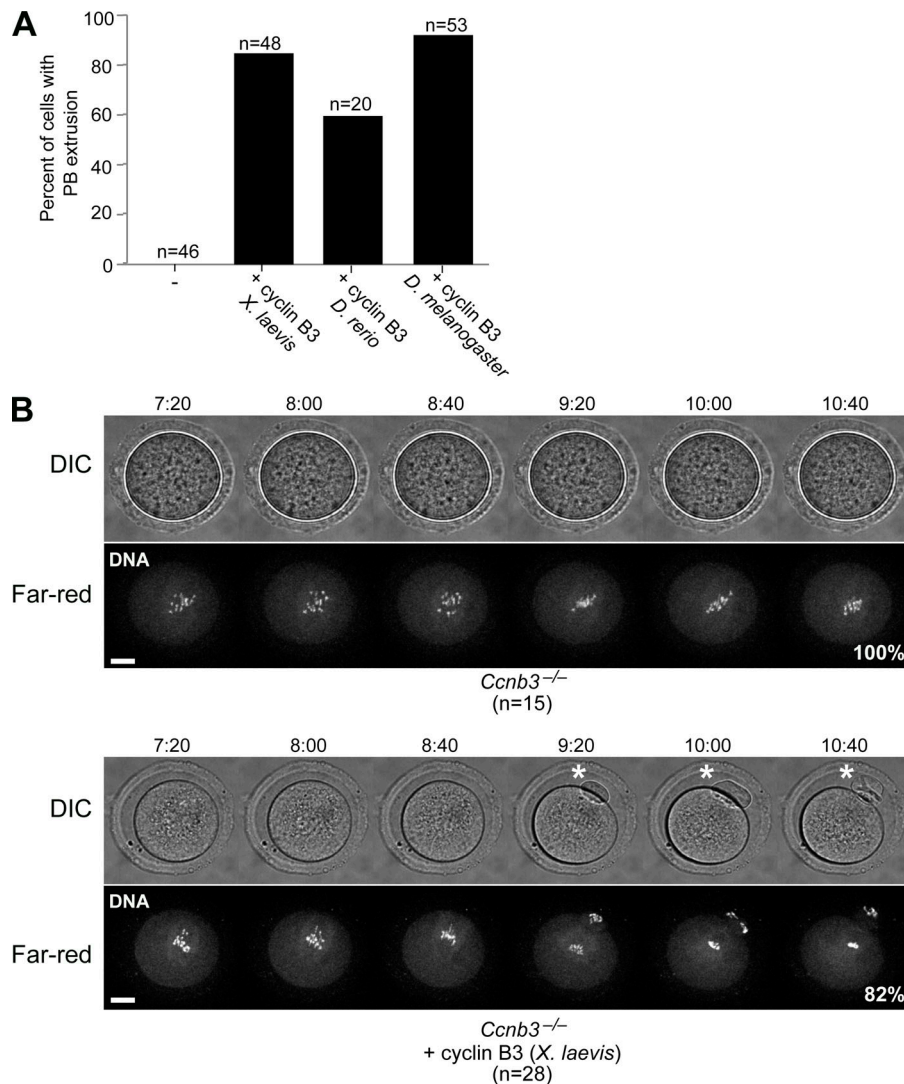
Figure 6. **Only cyclin B3 that can support in vitro kinase activity can rescue *Ccnb3*^{−/−} oocytes. (A)** Affinity purification of cyclin B3–CDK1 complexes. [MBPHis]cyclin B3 or [MBPHis]cyclin B3 MRL mutant were expressed in insect cells alone or coexpressed with either untagged or HA-tagged CDK1. Left: The eluates from purification on amylose resin were separated on SDS-PAGE and stained with Coomassie. Right: Representative autoradiograph (top) and quantification (bottom) from histone H1 kinase assays. In the graph, values in each experiment (n = 3) were normalized to the signal from the [MBPHis]cyclin B3 MRL sample (lane 4 in the autoradiograph); lines indicate means (lane 1: 1.733; lane 2: 4.351; lane 3: 3.878; lane 4: 0 [used for normalization]; lane 5: 0.121; lane 6: −0.202). **(B)** Rescue of *Ccnb3*^{−/−} oocytes by expression of exogenous cyclin B3. *Ccnb3*^{−/−} oocytes were sham injected or injected with the indicated cyclin mRNA, then released into meiosis I. Frames of representative videos are shown. Times after GVBD are indicated as hours:minutes, and percentages of oocytes of the shown phenotypes are indicated. Scale bar, 20 µm. White asterisks: PBs. n: number of oocytes from three independent experiments. **(C)** Total cyclin B–CDK1 activity during oocyte maturation, in control (lane 1–3), and *Ccnb3*^{−/−} (lanes 4–9, labeled in red) oocytes expressing wild-type cyclin B3 (lanes 6 and 7) or ΔDbox cyclin B3 (lanes 8 and 9), at the time points indicated as hours:minutes after GVBD. Oocytes extruding PBs are indicated. Histone H1 was used as a substrate. A representative example from two independent experiments is shown above; quantification of both experiments is shown below (^{32}P-H1 signal normalized to the signal in lane 2; points are values from each experiment; lines indicate means: lane 1: 6.61; lane 2: 100 [used for normalization]; lane 3: 14.38; lane 4: 191.58; lane 5: 138.53; lane 6: 109.88; lane 7: 9.59; lane 8: 37.36; lane 9: 1.5). **(D)** Representative chromosome spreads 16 h after GVBD. Chromosomes were stained with Hoechst (blue) and kinetochores with CREST (green). Insets show typical chromosome figures observed (chromosomes are shown in grayscale). Scale bar, 5 µm. n: number of oocytes from three independent experiments. Schematics of metaphase I bivalents or metaphase II univalent chromosomes are shown to aid interpretation.

Figure 7. Interspecies cross-complementation of Ccnb3^−/− oocytes. (A) Ccnb3^−/− oocytes were injected with the indicated mRNA, induced to enter meiosis I, and scored for PB extrusion. n: number of oocytes from three independent experiments; number of oocytes analyzed and percentage of PB extrusion: 46 Ccnb3^−/− sham injected oocytes (0% PBs), 48 Ccnb3^−/− oocytes injected with mRNA coding for *X. laevis* cyclin B3 (85.41%), 20 Ccnb3^−/− oocytes with *D. rerio* cyclin B3 mRNA (60%), and 53 Ccnb3^−/− oocytes with *D. melanogaster* cyclin B3 mRNA (92.45%). **(B)** Selected time frames of collapsed z-sections (12 sections, 3-μm steps) from a representative spinning disk confocal movie of Ccnb3^−/− sham-injected oocytes, and Ccnb3^−/− oocytes injected with *X. laevis* cyclin B3 mRNA. Before live imaging, oocytes were incubated with SiR-DNA. Top panel shows the DIC channel and bottom panel shows siR-DNA staining in far-red. Time points after GVBD are indicated as hours:minutes. Scale bar: 20 μm. White asterisks: PBs. n: number of oocytes from three independent experiments.

In principle, the failure of Ccnb3^−/− mutants to fully down-regulate steady-state cyclin B1 and securin levels could mean that cyclin B3–CDK1 represses translation of cyclin B1, securin, and/or other key cell cycle regulators. However, we think this is unlikely, as translation of transcripts coding for cyclin B1 and MOS is induced, not repressed, in a CDK1-dependent manner after GVBD (Han et al., 2017). Nevertheless, we cannot exclude a more indirect role of cyclin B3 in translational control.

We propose that cyclin B3 tips the balance from accumulation of cyclin B1–CDK1 activity toward APC/C-dependent degradation of cyclin B1 and progression into anaphase. Without cyclin B3, the APC/C is active, but endogenous cyclin B1 is not at all, and securin is not efficiently targeted for degradation. Consistent with this view, rescue of Ccnb3^−/− oocytes by artificially down-regulating cyclin B1–CDK1 activity with roscovitine indicates that sufficient separase is liberated from its inhibitory interaction with securin. Cyclin B3 in mammalian oocytes appears dispensable for turning off the SAC, unlike in *C. elegans* (Deyter et al., 2010). Cyclin B3–CDK1 complexes may foster full APC/C activity directly by modifying APC/C substrates, APC/C subunits, APC/C activators (CDC20 and CDH1), or some

combination (Alfieri et al., 2017). The robustness of the arrest is comparable to that observed when maintaining high cyclin B1 levels (e.g., with nondegradable cyclin B1; Herbert et al., 2003; Touati et al., 2012), but not SAC activation, which is transient (Touati and Wassmann, 2016).

Nevertheless, cyclin B3 is not strictly essential, in that some mice (~10% of those assayed thus far) harbored oocytes able to progress through meiosis I. This incomplete penetrance may reflect subtle variation (perhaps from strain background) in either the degree of APC/C activation or the threshold of APC/C activity needed for progression. Put another way, cyclin B3–deficient oocytes may occasionally achieve just enough APC/C activity during a critical time window to cross a threshold needed for the switch-like transition into anaphase I.

In budding and fission yeast, sequential substrate phosphorylation during cell cycle progression is thought to be primarily via changes in overall CDK activity as opposed to substrate specificities of different cyclins (Stern and Nurse, 1996; Coudreuse and Nurse, 2010; Bouchoux and Uhlmann, 2011; Uhlmann et al., 2011). Accordingly, the cell cycle can be driven by a single CDK–cyclin fusion complex in *S. pombe* (Coudreuse

and Nurse, 2010; Swaffer et al., 2016). In mouse, CDK1 is the only CDK essential for mitotic cell cycle progression per se (Santamaría et al., 2007). Loss of cyclin B2 does not affect viability or fertility, indicating that cyclin B1 is sufficient (Brandeis et al., 1998). It may thus seem surprising that cyclin B3 has such a specific role in oocyte meiosis that cannot be replaced by cyclin B1. Hence, cell cycle progression in meiosis appears to be specifically dependent on individual CDK complexes. This conclusion is further supported by the fact that loss of CDK2 does not affect somatic cells but leads to sterility due to failure to enter meiosis I (Ortega et al., 2003). Cell type specificity is also seen for cyclin A2, which is required in hematopoietic stem cells, fibroblasts, and female meiosis, but not in other tissues (Kalaszczynska et al., 2009; Touati et al., 2012; Zhang et al., 2017).

Overall, our data show that cyclin B3 is an M-phase cyclin with a singular role in oocyte meiosis, probably due to the specificities of meiotic cell cycle regulation in this huge cell. A key challenge now will be to determine whether APC/C activity or substrate accessibility is directly dependent on cyclin B3–CDK activity, and to define relevant phosphorylation targets needed for proper meiotic progression.

Materials and methods

Animals

Mice in the Keeney laboratory were maintained under regulatory standards approved by the Memorial Sloan-Kettering Cancer Center (MSKCC) Institutional Animal Care and Use Committee. Mice in the Wassmann laboratory were maintained according to current French guidelines in a conventional mouse facility (UMR7622), with authorization C 75-05-13. All experiments were subject to ethical review and approved by the French Ministry of Higher Education and Research (authorization no. B-75-1308). For this study, females were either purchased at 7 wk of age (CD-1 mice, Janvier Lab France) and used at 8–16 wk of age for experiments or bred in our animal facilities and used at 8–16 wk of age (*Ccnb3* mouse strain). Except for genotyping, the mice had not been involved in any procedures before experimentation, and they were given ad libitum access to food and water supply. The animals were housed under a 12-h light/12-h dark cycle according to the Federation of European Laboratory Science Associations.

Generation of *Ccnb3* knockout mouse strain, husbandry, and genotyping

Endonuclease mediated (*em*) allele was generated by the MSKCC Mouse Genetics Core Facility. Exon 7 of *Ccnb3* (National Center for Biotechnology Information [NCBI] gene ID: 209091) was targeted by guide RNA (C40-TGAACTTGGCATGATAGCAC). (Exon numbering used here is from the current accession. The targeted exon corresponds to exon 8 in the numbering used by Lozano et al. [2012].) Guide RNA was cloned into pDR274 vector for in vitro transcription. In vitro transcribed guide RNA (10 ng/µl) and Cas9 (20 ng/µl) were microinjected into pronuclei of CBA/J×C57BL/6J F2 hybrid zygotes using conventional techniques (Romanienko et al., 2016).

Genomic DNA from founder animals were subjected to PCR by using the following primers: CCN3B-A, 5′-GAGTATTAGCAC TGAGTCAGGGAC-3′, and CCN3B-B, 5′-GGAATACCTCAGTTT CTTTTGCAC-3′. T7 endonuclease I digestion was performed to identify the animals carrying indels. Because male animals have one copy of the X-linked *Ccnb3* gene, T7 assay on males was performed in the presence of wild-type genomic DNA.

To define the molecular nature of indels, genomic DNA from T7-positive animals was amplified using the primers indicated above. Amplified PCR fragments were used for TA Cloning (TA Cloning Kit with pCR 2.1 vector; Invitrogen). 10 white bacterial colonies were selected, inserts were sequenced, and the mutations were characterized as deletions, insertions, or substitutions. The *em1* allele, an out-of-frame deletion, was chosen to generate the *Ccnb3em1Sky* line. After two rounds of backcrossing to C57BL/6J, animals were interbred to generate homozygous and heterozygous female animals and hemizygous male animals. Primers for genotyping were GT4-F, 5′-TGTTGATGAAGAGGA ATTTTTCAAATCATTCCT-3′, and GT4-R, 5′-TTCTTTTGCACC CAGAGTTGACTTAAAG-3′. The amplified PCR product was subjected to *Bsr*I enzyme digestion (NEB). A *Bsr*I site is lost in the *em1* allele. Because *Ccnb3* is X-linked, no *Ccnb3*^{+/+} females can be obtained through crosses yielding homozygous *Ccnb3*^{−/−} mice. Therefore, we bred *Ccnb3*[−/Y] males with *Ccnb3*^{+/−} females to obtain *Ccnb3*^{−/−} and *Ccnb3*^{+/−} females to use as experimental mice and littermate controls, respectively.

Oocyte harvesting and in vitro culture

GV-stage oocytes were collected from ovaries of euthanized CD-1 mice or *Ccnb3*^{+/−} and *Ccnb3*^{−/−} mice aged 8–16 wk. Ovaries were transferred to drops of homemade M2 medium at 38°C and dissected to obtain oocytes. Oocytes were collected and isolated from follicular cells with mouth pipetting using torn-out Pasteur pipettes. For all microinjection experiments, ovaries and oocytes were incubated in drops of commercial M2 medium (Sigma-Aldrich) and kept at GV stage by the addition of dibutyl cyclic AMP (dbcAMP; Sigma-Aldrich) at 100 µg/ml final concentration. Oocytes undergoing GVBD within at most 90 min after ovary dissection or release from dbcAMP were used for experiments. For all experiments using *Ccnb3*^{−/−} mice, for every *Ccnb3*^{−/−} mouse at least five mature GVBD-stage oocytes were left untreated and released in parallel to control oocytes to ascertain that no PB extrusion occurred. In the rare cases where PB extrusion occurred in *Ccnb3*^{−/−} oocytes, the experiment was aborted and not taken into account (this was especially important for the rescue experiments in Figs. 3 E, 4 B, 6 [B–D], and 7 [A and B]). Where indicated, roscovitine was added 6:20 after GVDB at a final concentration of 0.2 mM, nocodazole at 6:00 after GVBD at a final concentration of 400 nM, and reversine at 6:40 after GVBD at a final concentration of 500 nM. Because it is soluble in oil, reversine was also added to the oil covering the media drops.

Histology

Ovaries from *Ccnb3*^{+/−} and *Ccnb3*^{−/−} adult mice were fixed overnight in 4% PFA at 4°C. Fixed tissues were washed in water and stored in 70% ethanol at 4°C. Fixed tissues were submitted to

Karasu et al.
Role of cyclin B3 in oocyte meiosis I

Journal of Cell Biology
https://doi.org/10.1083/jcb.201808091

1276

the Molecular Cytology Core Facility (MSKCC) for embedding in paraffin and sectioning of the embedded tissue (whole ovary) as 8-µm sections and preparation of slides with ovary sections. The slides were then subjected to immunohistochemistry as follows. The immunohistochemical staining was performed at the Molecular Cytology Core Facility (MSKCC) using a Discovery XT processor (Ventana Medical Systems). Ovary sections were deparaffinized with EZPrep buffer (Ventana Medical Systems), and antigen retrieval was performed with CC1 buffer (Ventana Medical Systems). Sections were blocked for 30 min with Background Buster solution (Innovex), followed by avidin-biotin blocking for 8 min (Ventana Medical Systems). Sections were then incubated with anti-VASA (ab13840; Abcam; 0.17 µg/ml) for 5 h, followed by 60-min incubation with biotinylated goat anti-rabbit (PK6101; Vector Labs) at 1:200 dilution. The detection was performed with DAB detection kit (Ventana Medical Systems) according to manufacturer instruction. Slides were counterstained with hematoxylin and coverslipped with Permount (Thermo Fisher Scientific). Immunohistochemistry slides were scanned using Pannoramic Flash 250 with a 20×/0.8 NA air objective. Images were analyzed using Pannoramic Viewer Software (3DHistech). To count oocytes, every fifth section on the slide was analyzed, and the number of oocytes in primordial, primary, secondary, and antral follicles were noted and summed.

Histological examination of somatic tissues

Gross histopathological analysis of major organs and tissues was performed by the MSKCC Laboratory of Comparative Pathology Core Facility for the following mice: two 2-mo-old $Ccnb3^{-/Y}$ males, one 2-mo-old $Ccnb3^{+/Y}$ male, two 5-mo-old $Ccnb3^{-/-}$ females, and two 5-mo-old $Ccnb3^{+/-}$ females. Histological examination of the following tissues was performed: diaphragm, skeletal muscle, sciatic nerve, heart/aorta, thymus, lung, kidneys, salivary gland, mesenteric lymph nodes, stomach, duodenum, pancreas, jejunum, ileum, cecum, colon, adrenals, liver, gallbladder, spleen, uterus, ovaries, cervix, urinary bladder, skin of dorsum and subjacent brown fat, skin of ventrum and adjacent mammary gland, thyroid, parathyroid, esophagus, trachea, stifle, sternum, coronal sections of head/brain, vertebrae, and spinal cord. Tissues were fixed in 10% neutral buffered formalin, and bones were decalcified in formic acid solution using the Surgipath Decalcifier I (Leica Biosystems) for 48 h. Samples were routinely processed in alcohol and xylene, embedded in paraffin, sectioned (5 µm), and stained with hematoxylin and eosin. Examined tissues and organs were grossly normal.

Extract preparation and Western blotting

To analyze endogenous protein levels, oocytes were cultured as described above. Oocytes were harvested at the indicated time points, washed in PBS to remove proteins from the medium, and then placed on the wall of the Eppendorf tube and snap-frozen in liquid nitrogen. Later, 7.5 µl of 1× Laemmli lysis buffer was added to the tube, and samples were boiled for 5 min at 100°C.

For Western blotting, samples were separated on 4–12% Bis-Tris NuPAGE precast gels (Life Technologies) at 150 V for 70 min. Proteins were transferred to PVDF membranes by wet transfer method in Tris-glycine-20% methanol, at 120 V for 40 min at 4°C. Membranes were blocked with 5% nonfat milk in PBS-0.1% Tween (PBS-T) for 30 min at room temperature on an orbital shaker. Blocked membranes were incubated with primary antibodies for 1 h at room temperature or overnight at 4°C. Membranes were washed with PBS-T for 30 min at room temperature, then incubated with HRP-conjugated secondary antibodies for 1 h at room temperature. Membranes were washed with PBS-T for 15 min and the signal was developed by ECL Plus Perkin Elmer or ECL Prime GE Healthcare.

To analyze cyclin B3 protein levels from mouse testis extracts, dissected testes were placed in an Eppendorf tube, frozen on dry ice, and stored at –80°C. The frozen tissue was resuspended in RIPA buffer (50 mM Tris-HCl, pH 7.5, 150 mM NaCl, 0.1% SDS, 0.5% sodium deoxycholate, and 1% NP-40) supplemented with protease inhibitors (Roche, Mini tablets). The tissue was disrupted with a plastic pestle and incubated by end-over-end rotation for 15 min, at 4°C. After brief sonication, samples were centrifuged at 15,000 rpm for 15 min. The cleared lysate was transferred to a new tube and used for immunoprecipitation. Whole-cell extract was precleared with protein G beads by end-over-end rotation for 1 h at 4°C. Anti-cyclin B3 monoclonal antibody (10 µg; Abmart; clone number 19584-1R1-3/C500_140905, raised against the epitope SNMEKEFILDIPNK [amino acids 110–123]) was then added to the precleared lysates and incubated overnight with end-over-end rotation, at 4°C. Protein G beads were added to the tubes and incubate for 1 h with end-over-end rotation, at 4°C. Beads were washed three times with RIPA buffer, resuspended in 1× NuPAGE LDS sample buffer (Invitrogen) with 50 mM DTT, and boiled for 5 min to elute immunoprecipitated proteins.

Primary antibodies were used at the following dilutions to detect proteins: mouse anti-securin (1:300; ab3305; Abcam), mouse anti-cyclin B1 (1:400; ab72; Abcam), mouse anti–β actin (1:1,000; 8H10D10; CST), mouse anti–cyclin B3 (1:500; Abmart), and rat anti–tubulin α (1:1,000; MCA78G; Bio-Rad). Secondary antibodies were used at the following dilutions: goat anti-mouse IgG (H+L)-HRP (1:10,000; 1721011; Bio-Rad), and goat anti-rat IgG-HRP (1:10,000; AP136P; Millipore).

Plasmids

Mouse $Ccnb3$ mRNA was amplified by PCR from a whole-testis cDNA library and cloned into pRN3-RFP vectors using the In-Fusion cloning kit (Clontech). $X.$ $laevis$ $cyclin$ $B3$ cDNA (clone ID: 781186; NCBI ID: 379048) was purchased from Dharmacon and used as a template for PCR amplification. $D.$ $rerio$ and $D.$ $melanogaster$ $cyclin$ $B3$ (NCBI ID: 767751 and 42971, respectively) were amplified by PCR from cDNA from $D.$ $rerio$ embryo or the S2 cell line, respectively. Amplified products for $X.$ $laevis$, $D.$ $rerio$, and $D.$ $melanogaster$ were cloned into pRN3-GFP vector using the In-Fusion cloning kit (Clontech). To generate $Ccnb3$ MRL mutation, overlapping primers with specific mutation were used to amplify PCR product from the wild-type template pRN3–cyclin B3–RFP, the template was digested by $DpnI$ treatment, and the PCR product was used to transform $Escherichia$ $coli$ DH5α competent cells. To generate the ΔD-box mutation, PCR primers that delete the D-box were used to amplify the $Ccnb3$ plasmid, and the

resulting PCR product was phosphorylated and ligated. The primer list can be found as Table S1. Plasmids for in vitro transcription of cyclin B1–GFP, securin-YFP, histone H2B-RFP, cyclin A2–GFP, and β-tubulin-GFP were used (Brunet et al., 1998; Herbert et al., 2003; Terret et al., 2003; Tsurumi et al., 2004; Touati et al., 2012).

Expression and purification of recombinant proteins

Vectors for expression of cyclin B3 (wild-type or MRL mutant) N-terminally tagged with maltose-binding protein and 6× histidine were generated by cloning in pFastBac1-MBP6XHis. Wild-type Ccnb3 was amplified from pRN3–cyclin B3–RFP and the MRL mutant was amplified from pRN3-cyclin B3 MRL-RFP. The plasmid was digested with SspI restriction endonucleases. By using In-Fusion cloning kit (Clontech) the PCR products were cloned into SspI linearized plasmid. Viruses were produced by a Bac-to-Bac Baculovirus Expression System (Invitrogen) following the manufacturer's instructions. Baculovirus expressing CDK1 and CDK1-HA were generously supplied by R. Fisher (Desai et al., 1992).

To express ^{MBPHis}cyclin B3 and ^{MBPHis}cyclin B3 MRL alone, Spodoptera frugiperda Sf9 cells were infected with virus at a multiplicity of infection (MOI) of 3. To express ^{MBPHis}cyclin B3–CDK1 or CDK1-HA and ^{MBPHis}cyclin B3 MRL-CDK1 or CDK1-HA complexes, Sf9 cells were infected with both viruses at an MOI of 3 and 2, respectively. Cells from two 150-mm plastic dishes per infection (each containing ∼3 × 10^7 cells) were harvested 48 h after infection by centrifugation at 1,500 rpm for 5 min and then washed with ice-cold PBS. Cell pellets were resuspended in 1.7 ml of ice-cold lysis buffer (25 mM Hepes-NaOH, pH 7.5, 150 mM NaCl, and 100 µM leupeptin; L2884; Sigma-Aldrich), 1× complete protease inhibitor tablet (Roche), and 0.5 mM PMSF. Cells were lysed by sonication and centrifuged at 15,000 rpm for 30 min, at 4°C. The cleared extract was moved to a 2-ml Eppendorf tube and mixed with 300 µl slurry of amylose resin (E802L; NEB) preequilibrated with lysis buffer. After 1 h at 4°C with end-over-end rotation, the amylose resin was centrifuged at 300 g for 1 min at 4°C. Resin was washed briefly with ice-cold lysis buffer before transfer on Bio-Spin chromatography columns (7326008; Bio-Rad). The resin on the column was washed five times with ice-cold wash buffer (lysis buffer plus 10% glycerol). To elute the proteins from the column, the resin was incubated with 100–200 µl ice-cold elution buffer (wash buffer plus 10 mM maltose [M5885; Sigma-Aldrich]). All steps during the purification were done at 4°C.

Histone H1 kinase assay with recombinant proteins expressed in Sf9 cells

Eluates from the amylose affinity purification step were used for histone H1 kinase assays. Reactions were performed in 10 mM Hepes-NaOH, pH 7.4, 75 mM NaCl, 1 mM DTT, 10 mM MgCl$_2$, 100 µM ATP (11140965001; Roche), 1 µCi [γ-^{32}P] ATP, and histone H1 (5 µg/µl; 10223549001; Sigma-Aldrich). 10 µl reaction mix was added to 10 µl eluate from the amylose resin and incubated for 30 min at room temperature. To terminate reactions, 5 µl of 4× SDS sample buffer was added to each reaction, and samples were boiled for 5 min before loading on 12% NuPage

Bis-Tris NuPAGE precast gels (Life Technologies). Samples were subjected to electrophoresis at 150 V for 60 min. The gel was then vacuum dried for 45 min at 80°C. Radiolabeled species were imaged using a Fuji phosphorimager and analyzed by Image Gauge software.

Histone H1 kinase assays using oocyte extracts

Kinase assays to determine endogenous kinase activity were performed on aliquots of five oocytes at the indicated stages of meiotic maturation (Kudo et al., 2006). In short, oocytes were lysed in 3 µl of lysis buffer (50 mM Tris, pH 7.5, 150 mM NaCl, 1% Igepal [Sigma-Aldrich], 10% glycerol, and 2 mM EDTA, supplemented with protease inhibitors [Mini tablets; Roche]) on ice for 20 min before adding 6 µl kinase assay buffer (50 mM Tris, pH 7.5, 150 mM NaCl, 10 mM MgCl$_2$, 0.5 mM DTT, 2.5 mM EGTA, and 150 µM ATP) supplemented with 3 µCi of [γ-^{32}P]ATP (Perkin Elmer) per sample. Histone H1 (0.5 µg per sample; Millipore) was used as a substrate. Kinase reactions were incubated 30 min at 30°C, denatured, and analyzed by SDS-PAGE. The gel was fixed and dried before being exposed and scanned to detect incorporation of [γ-^{32}P]ATP into the substrate, using a Typhoon FLA9000 phosphorimager (GE Healthcare Life Sciences). Scans were analyzed by ImageJ (National Institutes of Health).

Microinjection and live imaging

In vitro transcription of all mRNAs was done using the Ambion mMessage Machine kit according to the manufacturer's instructions. mRNAs (1 to 10 pM) were purified on RNeasy purification columns (Qiagen). GV stage oocytes were microinjected with mRNA on an inverted Nikon Eclipse Ti microscope. Microinjection pipettes were made using a magnetic puller (PN-30; Narishige). Oocytes were manipulated with a holding pipette (VacuTip; Eppendorf), and injection was done using a FemtoJet Microinjector pump (Eppendorf) with continuous flow. Injection of the oocytes was done on a Tokai Hit temperature controlled glass plate at 38°C. Live imaging of oocytes in Fig. 3 (B and E) and Fig. 7 B and Videos 1 and 2 was performed on an inverted Zeiss Axiovert 200M microscope coupled to an EMCCD camera (Evolve 512; Photometrics), combined with an MS-2000 automated stage (Applied Scientific Instrumentation), a Yokogawa CSU-X1 spinning disc, and a nanopositioner MCL Nano-Drive and using a Plan-APO (40×/1.4 NA) oil objective (Zeiss). Images of chromosomes were acquired with 11 z-sections of 3 µm, unless otherwise mentioned. For live imaging in Fig. 2 A; Fig. 3 F; Fig. 5, A–C; and Fig. 6 B, a Nikon eclipse TE 2000-E inverted microscope with motorized stage, equipped with PrecisExite High Power LED Fluorescence (LAM 1: 400/465, LAM 2: 585), a Märzhäuser Scanning Stage, a CoolSNAP HQ2 camera, and a Plan APO (20×/0.75 NA) objective was used. One section in z was acquired for all videos except videos for Fig. 2 A where 11 z-sections of 3 µm were acquired. Both microscopes were controlled by Metamorph software, and all live imaging was done in commercial M2 medium (Sigma-Aldrich), covered by mineral oil (embryo certified; Sigma-Aldrich) at 38°C. All images were stacked and assembled using ImageJ. Quantifications were done on untreated images. For figures, brightness was adjusted

with the same parameters per experimental condition with ImageJ.

Chromosome spreads and immunofluorescence

Oocytes were rinsed in successive drops of Tyrode's acid solution to remove their zona pellucida. For chromosome spreads, oocytes were fixed at room temperature using a spread solution (1% PFA, 0.15% Triton X-100, and 3 mM DTT; Sigma-Aldrich), at the time points indicated. For whole-mount immunofluorescence, chambers were coated with concanavalin A (Sigma-Aldrich) in M2 polyvinylpyrrolidone (0.1 mM; Merck-Millipore) medium, and oocytes were placed in the chambers and centrifuged at 1,400 rpm for 13 min at 38°C. Oocytes were then placed in a cold treatment solution (20 mM Hepes-NaOH and 1 mM MgCl$_2$, pH 7.4) on top of ice (4°C) for 4 min to remove unstable microtubules. After cold treatment, oocytes were incubated in a formaldehyde fixation solution (BRB80 medium with 0.3% Triton X-100 and 1.9% formaldehyde [Sigma-Aldrich]) at 38°C for 30 min. Primary antibodies were used at the indicated concentrations: human CREST serum autoimmune antibody against centromere (1:100; HCT-0100; Immunovision), rabbit polyclonal anti-MAD2 (1:50; Wassmann and Benezra, 1998), and mouse monoclonal anti–α-tubulin (DM1A) coupled to FITC (1:100; F2168; Sigma-Aldrich). Secondary antibodies were used at the following concentrations: anti-human Alexa Fluor 488 (1:200; A11013; Life Technologies), anti-human Cy3 (1:200; 709-166-149; Jackson ImmunoResearch), anti-rabbit Cy3 (1:200; 711-166-152; Jackson ImmunoResearch). Hoechst 3342 (H21492; Invitrogen) at 50 µg/ml was used to stain chromosomes, and AF1 Cityfluor mounting medium was used.

Image acquisitions of fixed oocytes

An inverted Zeiss Axiovert 200M microscope as described above for live imaging was used to image chromosome spreads and for whole-mount immunofluorescence acquisitions, using a 100×/1.4 NA oil objective coupled to an EMCCD camera (Evolve 512; Photometrics). Six z-sections of 0.4 µm were taken for spreads, and 11 z-sections of 1 µm for whole-mount oocytes. Stacks acquired with Metamorph software were assembled in ImageJ. Quantifications were done on untreated acquisitions. For figures, brightness was adjusted with the same parameters per experimental condition, using ImageJ.

Quantification of fluorescent signals

For the quantification of MAD2 fluorescence signal, the intensity was calculated for each kinetochore using an 8 × 8-pixel square on the kinetochore (where CREST signal is located). The same sized square was used adjacent to the MAD2 fluorescence to measure background, which was subtracted from the MAD2 signal. The MAD2 fluorescence intensity was normalized to the CREST signal of the same kinetochore. For the cyclin B3–RFP, ΔDbox cyclin B3–RFP, cyclin A2–GFP, cyclin B1–GFP, and securin-YFP quantifications, a 150 × 150-pixel circle was placed in the center of each oocyte for the fluorescence intensity signal measurement, and another was placed adjacent to the oocyte to measure background. For each oocyte, background-subtracted values were normalized relative to the highest value. All measurements were done using ImageJ on untreated acquisitions.

Statistical analysis

For statistical analysis, GraphPad Prism 7 was used. For the comparison of independent samples, unpaired Student's t test was performed. Error bars indicate means ± SD. Sample sizes and statistical tests are indicated in the figures and figure legends, respectively. Selection of oocytes for different conditions was at random. No statistical analysis was used to determine sample size. Collection and analysis of the data were not performed blind to the conditions of the experiments, and no data from experiments were excluded from analysis. The number of independent replicates is indicated in the figure legends.

Online supplemental material

Videos 1 and 2 show chromosome movements in a representative control and a *Ccnb3$^{−/−}$* oocyte, respectively. Table S1 provides sequence information for the primers used in this study.

References

Alfieri, C., S. Zhang, and D. Barford. 2017. Visualizing the complex functions and mechanisms of the anaphase promoting complex/cyclosome (APC/C). *Open Biol.* 7:170204. https://doi.org/10.1098/rsob.170204

Baltus, A.E., D.B. Menke, Y.C. Hu, M.L. Goodheart, A.E. Carpenter, D.G. de Rooij, and D.C. Page. 2006. In germ cells of mouse embryonic ovaries, the decision to enter meiosis precedes premeiotic DNA replication. *Nat. Genet.* 38:1430–1434. https://doi.org/10.1038/ng1919

Bendris, N., B. Lemmers, J.M. Blanchard, and N. Arsic. 2011. Cyclin A2 mutagenesis analysis: a new insight into CDK activation and cellular localization requirements. *PLoS One.* 6:e22879. https://doi.org/10.1371/journal.pone.0022879

Bolcun-Filas, E., V.D. Rinaldi, M.E. White, and J.C. Schimenti. 2014. Reversal of female infertility by Chk2 ablation reveals the oocyte DNA damage checkpoint pathway. *Science.* 343:533–536. https://doi.org/10.1126/science.1247671

Bouchoux, C., and F. Uhlmann. 2011. A quantitative model for ordered Cdk substrate dephosphorylation during mitotic exit. *Cell.* 147:803–814. https://doi.org/10.1016/j.cell.2011.09.047

Brandeis, M., I. Rosewell, M. Carrington, T. Crompton, M.A. Jacobs, J. Kirk, J. Gannon, and T. Hunt. 1998. Cyclin B2-null mice develop normally and are fertile whereas cyclin B1-null mice die in utero. *Proc. Natl. Acad. Sci. USA.* 95:4344–4349. https://doi.org/10.1073/pnas.95.8.4344

Brunet, S., Z. Polanski, M.H. Verlhac, J.Z. Kubiak, and B. Maro. 1998. Bipolar meiotic spindle formation without chromatin. *Curr. Biol.* 8:1231–1234. https://doi.org/10.1016/S0960-9822(07)00516-7

Coudreuse, D., and P. Nurse. 2010. Driving the cell cycle with a minimal CDK control network. *Nature.* 468:1074–1079. https://doi.org/10.1038/nature09543

Davey, N.E., and D.O. Morgan. 2016. Building a Regulatory Network with Short Linear Sequence Motifs: Lessons from the Degrons of the Anaphase-Promoting Complex. *Mol. Cell.* 64:12–23. https://doi.org/10.1016/j.molcel.2016.09.006

Desai, D., Y. Gu, and D.O. Morgan. 1992. Activation of human cyclin-dependent kinases in vitro. *Mol. Biol. Cell.* 3:571–582. https://doi.org/10.1091/mbc.3.5.571

Deyter, G.M., T. Furuta, Y. Kurasawa, and J.M. Schumacher. 2010. Caenorhabditis elegans cyclin B3 is required for multiple mitotic processes including alleviation of a spindle checkpoint-dependent block in anaphase chromosome segregation. *PLoS Genet.* 6:e1001218. https://doi.org/10.1371/journal.pgen.1001218

Di Giacomo, M., M. Barchi, F. Baudat, W. Edelmann, S. Keeney, and M. Jasin. 2005. Distinct DNA-damage-dependent and -independent responses drive the loss of oocytes in recombination-defective mouse mutants. *Proc. Natl. Acad. Sci. USA.* 102:737–742. https://doi.org/10.1073/pnas.0406212102

El Yakoubi, W., and K. Wassmann. 2017. Meiotic Divisions: No Place for Gender Equality. *Adv. Exp. Med. Biol.* 1002:1–17. https://doi.org/10.1007/978-3-319-57127-0_1

Fisher, D., L. Krasinska, D. Coudreuse, and B. Novák. 2012. Phosphorylation network dynamics in the control of cell cycle transitions. *J. Cell Sci.* 125:4703–4711. https://doi.org/10.1242/jcs.106351

Gallant, P., and E.A. Nigg. 1994. Identification of a novel vertebrate cyclin: cyclin B3 shares properties with both A- and B-type cyclins. *EMBO J.* 13:595–605. https://doi.org/10.1002/j.1460-2075.1994.tb06297.x

Gui, L., and H. Homer. 2012. Spindle assembly checkpoint signalling is uncoupled from chromosomal position in mouse oocytes. *Development.* 139:1941–1946. https://doi.org/10.1242/dev.078352

Gunbin, K.V., V.V. Suslov, I.I. Turnaev, D.A. Afonnikov, and N.A. Kolchanov. 2011. Molecular evolution of cyclin proteins in animals and fungi. *BMC Evol. Biol.* 11:224. https://doi.org/10.1186/1471-2148-11-224

Han, S.J., J.P.S. Martins, Y. Yang, M.K. Kang, E.M. Daldello, and M. Conti. 2017. The Translation of Cyclin B1 and B2 is Differentially Regulated during Mouse Oocyte Reentry into the Meiotic Cell Cycle. *Sci. Rep.* 7:14077. https://doi.org/10.1038/s41598-017-13688-3

Heim, A., B. Rymarczyk, and T.U. Mayer. 2017. Regulation of Cell Division. *Adv. Exp. Med. Biol.* 953:83–116. https://doi.org/10.1007/978-3-319-46095-6_3

Hellmuth, S., F. Böttger, C. Pan, M. Mann, and O. Stemmann. 2014. PP2A delays APC/C-dependent degradation of separase-associated but not free securin. *EMBO J.* 33:1134–1147. https://doi.org/10.1002/embj.201488098

Herbert, M., M. Levasseur, H. Homer, K. Yallop, A. Murdoch, and A. McDougall. 2003. Homologue disjunction in mouse oocytes requires proteolysis of securin and cyclin B1. *Nat. Cell Biol.* 5:1023–1025. https://doi.org/10.1038/ncb1062

Herbert, M., D. Kalleas, D. Cooney, M. Lamb, and L. Lister. 2015. Meiosis and maternal aging: insights from aneuploid oocytes and trisomy births. *Cold Spring Harb. Perspect. Biol.* 7:a017970. https://doi.org/10.1101/cshperspect.a017970

Hochegger, H., A. Klotzbücher, J. Kirk, M. Howell, K. le Guellec, K. Fletcher, T. Duncan, M. Sohail, and T. Hunt. 2001. New B-type cyclin synthesis is required between meiosis I and II during Xenopus oocyte maturation. *Development.* 128:3795–3807.

Holt, J.E., S.I. Lane, and K.T. Jones. 2013. The control of meiotic maturation in mammalian oocytes. *Curr. Top. Dev. Biol.* 102:207–226. https://doi.org/10.1016/B978-0-12-416024-8.00007-6

Holt, L.J., A.N. Krutchinsky, and D.O. Morgan. 2008. Positive feedback sharpens the anaphase switch. *Nature.* 454:353–357. https://doi.org/10.1038/nature07050

Jacobs, H.W., J.A. Knoblich, and C.F. Lehner. 1998. Drosophila Cyclin B3 is required for female fertility and is dispensable for mitosis like Cyclin B. *Genes Dev.* 12:3741–3751. https://doi.org/10.1101/gad.12.23.3741

Jain, D., M.R. Puno, C. Meydan, N. Lailler, C.E. Mason, C.D. Lima, K.V. Anderson, and S. Keeney. 2018. *ketu* mutant mice uncover an essential meiotic function for the ancient RNA helicase YTHDC2. *eLife.* 7:e30919. https://doi.org/10.7554/eLife.30919

Jeffrey, P.D., A.A. Russo, K. Polyak, E. Gibbs, J. Hurwitz, J. Massagué, and N.P. Pavletich. 1995. Mechanism of CDK activation revealed by the structure of a cyclinA-CDK2 complex. *Nature.* 376:313–320. https://doi.org/10.1038/376313a0

Kalaszczynska, I., Y. Geng, T. Iino, S. Mizuno, Y. Choi, I. Kondratiuk, D.P. Silver, D.J. Wolgemuth, K. Akashi, and P. Sicinski. 2009. Cyclin A is redundant in fibroblasts but essential in hematopoietic and embryonic stem cells. *Cell.* 138:352–365. https://doi.org/10.1016/j.cell.2009.04.062

Kubiak, J.Z., M. Weber, G. Géraud, and B. Maro. 1992. Cell cycle modification during the transitions between meiotic M-phases in mouse oocytes. *J. Cell Sci.* 102:457–467.

Kudo, N.R., K. Wassmann, M. Anger, M. Schuh, K.G. Wirth, H. Xu, W. Helmhart, H. Kudo, M. McKay, B. Maro, et al. 2006. Resolution of chiasmata in oocytes requires separase-mediated proteolysis. *Cell.* 126:135–146. https://doi.org/10.1016/j.cell.2006.05.033

Lane, S.I., Y. Yun, and K.T. Jones. 2012. Timing of anaphase-promoting complex activation in mouse oocytes is predicted by microtubule-kinetochore attachment but not by bivalent alignment or tension. *Development.* 139:1947–1955. https://doi.org/10.1242/dev.077040

Ledan, E., Z. Polanski, M.E. Terret, and B. Maro. 2001. Meiotic maturation of the mouse oocyte requires an equilibrium between cyclin B synthesis

and degradation. *Dev. Biol.* 232:400–413. https://doi.org/10.1006/dbio .2001.0188

Li, X.C., and J.C. Schimenti. 2007. Mouse pachytene checkpoint 2 (trip13) is required for completing meiotic recombination but not synapsis. *PLoS Genet.* 3:e130. https://doi.org/10.1371/journal.pgen.0030130

Li, J., J.X. Tang, J.M. Cheng, B. Hu, Y.Q. Wang, B. Aalia, X.Y. Li, C. Jin, X.X. Wang, S.L. Deng, et al. 2018a. Cyclin B2 can compensate for Cyclin B1 in oocyte meiosis I. *J. Cell Biol.* 217:3901–3911. https://doi.org/10.1083/jcb .201802077

Li, Y., L. Wang, L. Zhang, Z. He, G. Feng, H. Sun, J. Wang, Z. Li, C. Liu, J. Han, et al. 2018b. Cyclin B3 is specifically required for metaphase to anaphase transition in mouse oocyte meiosis I. *bioRxiv.* doi: (Preprint posted August 20, 2018). https://doi.org/10.1101/390351

Lischetti, T., and J. Nilsson. 2015. Regulation of mitotic progression by the spindle assembly checkpoint. *Mol. Cell. Oncol.* 2:e970484. https://doi .org/10.4161/23723548.2014.970484

Lozano, J.C., V. Vergé, P. Schatt, J.L. Juengel, and G. Peaucellier. 2012. Evolution of cyclin b3 shows an abrupt three-fold size increase, due to the extension of a single exon in placental mammals, allowing for new protein-protein interactions. *Mol. Biol. Evol.* 29:3855–3871. https://doi .org/10.1093/molbev/mss189

Malumbres, M., E. Harlow, T. Hunt, T. Hunter, J.M. Lahti, G. Manning, D.O. Morgan, L.H. Tsai, and D.J. Wolgemuth. 2009. Cyclin-dependent kinases: a family portrait. *Nat. Cell Biol.* 11:1275–1276. https://doi.org/ 10.1038/ncb1109-1275

Meijer, L., A. Borgne, O. Mulner, J.P. Chong, J.J. Blow, N. Inagaki, M. Inagaki, J.G. Delcros, and J.P. Moulinoux. 1997. Biochemical and cellular effects of roscovitine, a potent and selective inhibitor of the cyclin-dependent kinases cdc2, cdk2 and cdk5. *Eur. J. Biochem.* 243:527–536. https://doi .org/10.1111/j.1432-1033.1997.t01-2-00527.x

Miles, D.C., J.A. van den Bergen, A.H. Sinclair, and P.S. Western. 2010. Regulation of the female mouse germ cell cycle during entry into meiosis. *Cell Cycle.* 9:408–418. https://doi.org/10.4161/cc.9.2.10691

Morgan, D.O. 1997. Cyclin-dependent kinases: engines, clocks, and microprocessors. *Annu. Rev. Cell Dev. Biol.* 13:261–291. https://doi.org/10.1146/ annurev.cellbio.13.1.261

Nguyen, T.B., K. Manova, P. Capodieci, C. Lindon, S. Bottega, X.Y. Wang, J. Refik-Rogers, J. Pines, D.J. Wolgemuth, and A. Koff. 2002. Characterization and expression of mammalian cyclin b3, a prepachytene meiotic cyclin. *J. Biol. Chem.* 277:41960–41969. https://doi.org/10.1074/jbc.M203951200

Niault, T., K. Hached, R. Sotillo, P.K. Sorger, B. Maro, R. Benezra, and K. Wassmann. 2007. Changing Mad2 levels affects chromosome segregation and spindle assembly checkpoint control in female mouse meiosis I. *PLoS One.* 2:e1165. https://doi.org/10.1371/journal.pone.0001165

Nieduszynski, C.A., J. Murray, and M. Carrington. 2002. Whole-genome analysis of animal A- and B-type cyclins. *Genome Biol.* 3:research0070.1. https://doi.org/10.1186/gb-2002-3-12-research0070

Nikalayevich, E., N. Bouftas, and K. Wassmann. 2018. Detection of Separase Activity Using a Cleavage Sensor in Live Mouse Oocytes. *Methods Mol. Biol.* 1818:99–112. https://doi.org/10.1007/978-1-4939-8603-3_11

Ortega, S., I. Prieto, J. Odajima, A. Martín, P. Dubus, R. Sotillo, J.L. Barbero, M. Malumbres, and M. Barbacid. 2003. Cyclin-dependent kinase 2 is essential for meiosis but not for mitotic cell division in mice. *Nat. Genet.* 35:25–31. https://doi.org/10.1038/ng1232

Petronczki, M., M.F. Siomos, and K. Nasmyth. 2003. Un ménage à quatre: the molecular biology of chromosome segregation in meiosis. *Cell.* 112: 423–440. https://doi.org/10.1016/S0092-8674(03)00083-7

Rattani, A., P.K. Vinod, J. Godwin, K. Tachibana-Konwalski, M. Wolna, M. Malumbres, B. Novák, and K. Nasmyth. 2014. Dependency of the spindle assembly checkpoint on Cdk1 renders the anaphase transition irreversible. *Curr. Biol.* 24:630–637. https://doi.org/10.1016/j.cub.2014 .01.033

Refik-Rogers, J., K. Manova, and A. Koff. 2006. Misexpression of cyclin B3 leads to aberrant spermatogenesis. *Cell Cycle.* 5:1966–1973. https://doi .org/10.4161/cc.5.17.3137

Romanienko, P.J., J. Giacalone, J. Ingenito, Y. Wang, M. Isaka, T. Johnson, Y. You, and W.H. Mark. 2016. A vector with a single promoter for *in vitro* transcription and mammalian cell expression of CRISPR gRNAs. *PLoS One.* 11:e0148362. https://doi.org/10.1371/journal.pone.0148362

Santaguida, S., A. Tighe, A.M. D'Alise, S.S. Taylor, and A. Musacchio. 2010. Dissecting the role of MPS1 in chromosome biorientation and the spindle checkpoint through the small molecule inhibitor reversine. *J. Cell Biol.* 190:73–87. https://doi.org/10.1083/jcb.201001036

Santamaría, D., C. Barrière, A. Cerqueira, S. Hunt, C. Tardy, K. Newton, J.F. Cáceres, P. Dubus, M. Malumbres, and M. Barbacid. 2007. Cdk1 is

sufficient to drive the mammalian cell cycle. *Nature.* 448:811–815. https://doi.org/10.1038/nature06046

Schulman, B.A., D.L. Lindstrom, and E. Harlow. 1998. Substrate recruitment to cyclin-dependent kinase 2 by a multipurpose docking site on cyclin A. *Proc. Natl. Acad. Sci. USA.* 95:10453–10458. https://doi.org/10.1073/ pnas.95.18.10453

Shindo, N., K. Kumada, and T. Hirota. 2012. Separase sensor reveals dual roles for separase coordinating cohesin cleavage and cdk1 inhibition. *Dev. Cell.* 23:112–123. https://doi.org/10.1016/j.devcel.2012.06.015

Sigrist, S., H. Jacobs, R. Stratmann, and C.F. Lehner. 1995. Exit from mitosis is regulated by Drosophila fizzy and the sequential destruction of cyclins A, B and B3. *EMBO J.* 14:4827–4838. https://doi.org/10.1002/j.1460-2075 .1995.tb00164.x

Stemmann, O., I.H. Gorr, and D. Boos. 2006. Anaphase topsy-turvy: Cdk1 a securin, separase a CKI. *Cell Cycle.* 5:11–13. https://doi.org/10.4161/cc.5.1.2296

Stern, B., and P. Nurse. 1996. A quantitative model for the cdc2 control of S phase and mitosis in fission yeast. *Trends Genet.* 12:345–350. https://doi .org/10.1016/S0168-9525(96)80016-3

Swaffer, M.P., A.W. Jones, H.R. Flynn, A.P. Snijders, and P. Nurse. 2016. CDK substrate phosphorylation and ordering the cell cycle. *Cell.* 167: 1750–1761.e16. https://doi.org/10.1016/j.cell.2016.11.034

Tang, J.X., D. Chen, S.L. Deng, J. Li, Y. Li, Z. Fu, X.X. Wang, Y. Zhang, S.R. Chen, and Y.X. Liu. 2018. CRISPR/Cas9-mediated gene editing induces gene knockdown by altering the pre-mRNA splicing in mice. *BMC Biotechnol.* 18:61. https://doi.org/10.1186/s12896-018-0472-8

Terret, M.E., K. Wassmann, I. Waizenegger, B. Maro, J.M. Peters, and M.H. Verlhac. 2003. The meiosis I-to-meiosis II transition in mouse oocytes requires separase activity. *Curr. Biol.* 13:1797–1802. https://doi.org/10 .1016/j.cub.2003.09.032

Touati, S.A., and K. Wassmann. 2016. How oocytes try to get it right: spindle checkpoint control in meiosis. *Chromosoma.* 125:321–335. https://doi .org/10.1007/s00412-015-0536-7

Touati, S.A., D. Cladière, L.M. Lister, I. Leontiou, J.P. Chambon, A. Rattani, F. Böttger, O. Stemmann, K. Nasmyth, M. Herbert, and K. Wassmann. 2012. Cyclin A2 is required for sister chromatid segregation, but not separase control, in mouse oocyte meiosis. *Cell Reports.* 2:1077–1087. https://doi.org/10.1016/j.celrep.2012.10.002

Touati, S.A., E. Buffin, D. Cladière, K. Hached, C. Rachez, J.M. van Deursen, and K. Wassmann. 2015. Mouse oocytes depend on BubR1 for proper chromosome segregation but not for prophase I arrest. *Nat. Commun.* 6: 6946. https://doi.org/10.1038/ncomms7946

Treen, N., T. Heist, W. Wang, and M. Levine. 2018. Depletion of Maternal Cyclin B3 Contributes to Zygotic Genome Activation in the Ciona Embryo. *Curr. Biol.* 28:1330–1331. https://doi.org/10.1016/j.cub.2018.03.058

Tsurumi, C., S. Hoffmann, S. Geley, R. Graeser, and Z. Polanski. 2004. The spindle assembly checkpoint is not essential for CSF arrest of mouse oocytes. *J. Cell Biol.* 167:1037–1050. https://doi.org/10.1083/jcb.200405165

Uhlmann, F., C. Bouchoux, and S. López-Avilés. 2011. A quantitative model for cyclin-dependent kinase control of the cell cycle: revisited. *Philos. Trans. R. Soc. Lond. B Biol. Sci.* 366:3572–3583. https://doi.org/10.1098/rstb.2011.0082

van der Voet, M., M.A. Lorson, D.G. Srinivasan, K.L. Bennett, and S. van den Heuvel. 2009. C. elegans mitotic cyclins have distinct as well as overlapping functions in chromosome segregation. *Cell Cycle.* 8:4091–4102. https://doi.org/10.4161/cc.8.24.10171

Wassmann, K., and R. Benezra. 1998. Mad2 transiently associates with an APC/p55Cdc complex during mitosis. *Proc. Natl. Acad. Sci. USA.* 95: 11193–11198. https://doi.org/10.1073/pnas.95.19.11193

Wassmann, K., T. Niault, and B. Maro. 2003. Metaphase I arrest upon activation of the Mad2-dependent spindle checkpoint in mouse oocytes. *Curr. Biol.* 13:1596–1608. https://doi.org/10.1016/j.cub.2003.08.052

Yang, Y., C.R. Yang, S.J. Han, E.M. Daldello, A. Cho, J.P.S. Martins, G. Xia, and M. Conti. 2017. Maternal mRNAs with distinct 3′ UTRs define the temporal pattern of Ccnb1 synthesis during mouse oocyte meiotic maturation. *Genes Dev.* 31:1302–1307. https://doi.org/10.1101/gad.296871.117

Yuan, K., and P.H. O'Farrell. 2015. Cyclin B3 is a mitotic cyclin that promotes the metaphase-anaphase transition. *Curr. Biol.* 25:811–816. https://doi .org/10.1016/j.cub.2015.01.053

Zhang, Q.H., W.S. Yuen, D. Adhikari, J.A. Flegg, G. FitzHarris, M. Conti, P. Sicinski, I. Nabti, P. Marangos, and J. Carroll. 2017. Cyclin A2 modulates kinetochore-microtubule attachment in meiosis II. *J. Cell Biol.* 216: 3133–3143. https://doi.org/10.1083/jcb.201607111

Zhang, T., S.T. Qi, L. Huang, X.S. Ma, Y.C. Ouyang, Y. Hou, W. Shen, H. Schatten, and Q.Y. Sun. 2015. Cyclin B3 controls anaphase onset independent of spindle assembly checkpoint in meiotic oocytes. *Cell Cycle.* 14:2648–2654. https://doi.org/10.1080/15384101.2015.1064567